‘Hourglass control in non-linear finite element analysis,using hexahedral elements’

Thesis of Stavros Ntioudis

University of Thessaly

Laboratory of mechanics and strength of materials

Departement of Mechanical Engineering

Volos, Greece

Hourglass control in non-linear finite element analysis,using hexahedral elements

Author:
Stavros Ntioudis

Supervisor:
Prof. Nikolaos Aravas

October 12, 2018

UNIVERSITY OF
THESSALY

Contents

Introduction

A gradient-enhanced elastoplasticity model is introduced in the direction of circumventing the numerous-negative analysis accuracy issues linked to the finite element modeling of failure mechanisms of ductile metals. In addition, an enhanced assumed strain (EAS) hourglass control theory is developed for the purpose of addressing the numerical phenomenon of zero-energy modes - a phenomenon which often leads to an approximate solution with no physical meaning. Later, the (EAS) model is implemented in a reduced-integrated non-linear (gradient-enhanced), hexahedral finite element which is eventually "imported" to the commercial finite element analysis software "ABAQUS", with the programming of a proper user element subroutine.

Of course this provided us with the opportunity of exploiting the explicit as well as implicit solvers of "ABAQUS" in order to perform F.E. analyses using our newly proposed brick. Ultimately, in a series of demanding patch problems, the user element is examined thoroughly and its accuracy as well as simulation convergence rate are measured, evaluated and compared with relevant simulation results of various other commercial elements. This thesis aims to familiarize the reader with the difficulties of hourglass control as well as the practical and theoretical challenges of finite element formulation in the non-linear regime and certainly demonstrates a systematic approach of F.E. efficiency estimation with a comprehensive element testing problem set.

Theoretical Section

The first part of this particular section contains a summary of the constitutive model theory implemented in our non-linear, hexahedral finite element. Then follows a brief discussion concerning the concept of reduced integration schemes as well as hourglass modes and ultimately, in the context of the last theoretical subsection, the ideas of hourglass control and specifically those of the enhanced assumed strain techniques are thoroughly explained.

2.1 Constitutive model: Gradient-enhanced elastoplasticity for softening behaviour

2.1.1 Introduction to elastoplastic models for softening behavior

For years, various researchers have been focusing their efforts on the numerical modeling of failure mechanisms of engineering materials. Especially for the case of ductile materials in the non-linear regime, a great challenge rises due to the fact that their deformation is intensively localized into a narrow zone - a zone whose thickness is determined by the underlying microstructure of the material. Of course, the characteristic softening response in plastically deforming solids and eventually the formation of shear bands lead to an ill-condition where the finite element solution strongly depends on the direction and the fineness of the selected computational mesh. From a mathematical point of view the boundary value problem loses ellipticity in statics (or hyperbolicity in dynamics) and ultimately the deformation tends to localize into a singularity.

In the direction of circumventing the critical (for the accuracy of the finite element analysis) issue stated above, different theories have been developed during the past decades, with the most common of them being the high-order continuum based models (Aifantis E. C. (a) ,Aifantis E. C. (b) ; Stolken J. S. and Evans A. G.; Shu J. Y. and Barlow C. Y.) as well as the non local plasticity models(Strömberg L. and Ristinmaa M.; Nilsson C.). The later ones introduce a nonlocal quantity which is defined as the spatially weighted average of the local values of plastic deformation (non local plastic deformation), however these models tend to be computationally inefficient as the non local variable which "measures" the plasticity length scale gets computed in an integral format.

The USER element presented in the context of this thesis utilizes a gradient-enhanced plasticity formulation (e.g. de Borst R. and Mühlaus H. B.), a theory which is essentially an extension-upgrade of the nonlocal plasticity models with the nonlocal quantity being computed with a Taylor series approximation instead of the integral format. Of course, in contrast with the 'explicit' gradient-enhanced formulations which are directly using the high-order gradient terms of the non local quantity, an 'implicit' format which exploits the high-order derivatives of the nonlocal value is implemented in our USER element.

2.1.2 General isotropic plasticity model with damage

Following the introduction to gradient-enhanced elastoplasticity models and in the context of the following subsections, the basic equations integrated in our ABAQUS USER subroutines are presented in detail.

To begin with we can express the yield function as:

$$\Phi = \hat{\Phi}\left(I_1, J_2, J_3, \bar{\varepsilon}^p\right) = \tilde{\Phi}\left(p, \sigma_e, \theta, \bar{\varepsilon}^p\right) \tag{2.1}$$

where

$$p = \frac{\sigma_{kk}}{3} = \frac{I_1}{3} \tag{2.2}$$

$$\sigma_e = \sqrt{\frac{3}{2} s_{ij}\, s_{ij}} = \sqrt{3\, J_2} \tag{2.3}$$

$$\sin 3\,\theta = -\frac{27}{2}\frac{J_3}{\sigma_e^3} \qquad \left(-\frac{\pi}{2} \leq 3\,\theta \leq \frac{\pi}{2}\right) \tag{2.4}$$

and

$$J_3 = \frac{1}{3}\mathrm{tr}\left(\mathbf{s}^3\right) = \det \mathbf{s} \tag{2.5}$$

Note that $J_3 = 0 \Leftrightarrow \theta = 0$

2.1.3 Gradient Plasticity with damage

The constitutive equations for our model can be defined as follows:

$$\mathbf{D} = \mathbf{D}^e + \mathbf{D}^p \tag{2.6}$$

$$\mathbf{D}^e = \mathbf{M}^e : \boldsymbol{\sigma} \tag{2.7}$$

$$\mathbf{D}^p = \dot{\lambda}\, \mathbf{P} \tag{2.8}$$

$$\mathbf{P} = \frac{\partial \Phi}{\partial \boldsymbol{\sigma}} \tag{2.9}$$

$$\dot{\bar{\varepsilon}}^p = \sqrt{\frac{2}{3}\mathbf{D}^p : \mathbf{D}^p} = \dot{\lambda}\bar{P} \tag{2.10}$$

and of course

$$\bar{P} = \sqrt{\frac{2}{3}\mathbf{P} : \mathbf{P}} \tag{2.11}$$

at this stage we can express the yield function implemented in our model as:

$$\Phi\left(\boldsymbol{\sigma}, \bar{\varepsilon}^p, e^p\right) = \sigma_e - \left[1 - \mathbf{D}\left(e^p\right)\right] F\left(\theta\right) \sigma_Y\left(\bar{\varepsilon}^p\right) = 0 \tag{2.12}$$

and note that:

$$e^p - \ell^2\, \nabla^2 e^p = \bar{\varepsilon}^p \quad or \quad e^p - \bar{\varepsilon}^p = \ell^2\, \nabla^2 e^p \tag{2.13}$$

with $\frac{\partial e^p}{\partial n} = 0$ on S

Acknowledge that if $\nabla^2 e^p = 0$, then $e^p = \bar{\varepsilon}^p$

Also:

$$\mathbf{P} = \frac{1}{3}\frac{\partial \Phi}{\partial p}\boldsymbol{\delta} + \frac{\partial \Phi}{\partial \sigma_e}\mathbf{N} + \frac{1}{\sigma_e}\frac{\partial \Phi}{\partial \theta}\mathbf{M} = \mathbf{N} + \left[1 - \mathbf{D}\left(e^p\right)\right]\frac{dF\left(\theta\right)}{d\theta}\frac{\sigma_Y\left(\bar{\varepsilon}^p\right)}{\sigma_e}\mathbf{M} \tag{2.14}$$

thus:

$$\frac{\partial \mathbf{P}}{\partial \bar{\varepsilon}^p} = \left[1 - \mathbf{D}\left(e^p\right)\right] \frac{dF\left(\theta\right)}{d\theta} \frac{h\left(\bar{\varepsilon}^p\right)}{\sigma_e} \mathbf{M} \quad and \quad \frac{\partial \mathbf{P}}{\partial e^p} = -\frac{d\mathbf{D}}{de^p} \frac{dF}{d\theta} \frac{\sigma_Y}{\sigma_e} \mathbf{M} \tag{2.15}$$

with

$$h\left(\bar{\varepsilon}^p\right) = \frac{d\sigma_Y\left(\bar{\varepsilon}^p\right)}{d\bar{\varepsilon}^p} \tag{2.16}$$

We can now define the boundary value problem

$$equilibrium: \qquad \sigma_{ij,j} + \rho\, b_i = 0 \tag{2.17}$$

$$kinematics: \qquad D_{ij} = \frac{1}{2}\left(u_{i,j} + u_{j,i}\right) \tag{2.18}$$

$$constitutive: \qquad \mathbf{D} = \mathbf{D}^e + \mathbf{D}^p \tag{2.19}$$

$$\mathbf{D}^e = \mathbf{M}^e : \boldsymbol{\sigma}, \qquad \mathbf{M}^e = \frac{1}{2\,G}\mathbf{K} + \frac{1}{3\,\kappa}\mathbf{J} \tag{2.20}$$

$$\mathbf{D}^p = \dot{\lambda}\mathbf{P} \quad \mathbf{P} = \frac{\partial \Phi}{\partial \sigma} \quad \dot{\bar{\varepsilon}}^p = \sqrt{\frac{2}{3}\mathbf{D}^p : \mathbf{D}^p} = \dot{\lambda}\bar{P} \quad \bar{P} = \sqrt{\frac{2}{3}\mathbf{P} : \mathbf{P}} \tag{2.21}$$

$$\Phi\left(\boldsymbol{\sigma}, \bar{\varepsilon}^p, e^p\right) = 0 \tag{2.22}$$

$$e^p - \ell^2\, \nabla^2 e^p = \bar{\varepsilon}^p \tag{2.23}$$

Finally, we apply the following boundary conditions:

$$u_i = \hat{u}_i \quad on \quad S_u \tag{2.24}$$

$$\sigma_{ij}\, n_j = \hat{t}_i \quad on \quad S_t \quad \left(S_u \cup S_t = S, S_u \cap S_t = \emptyset\right) \tag{2.25}$$

$$\frac{\partial e^p}{\partial n} = \frac{\partial e^p}{\partial x_i} n_i = 0 \quad on \quad S \tag{2.26}$$

Of course our gradient plasticity model is defined with the nodal displacements u_i as well as the non local plastic deformation e^p treated as primary unknowns and the integral statement for our given problem is expressed as:

$$\int_V \left[\sigma_{ij,j}\left(\mathbf{u}, e^p\right) + \rho\, b_i\right] u_i^*\, dV + \int_{S_t} \left[\sigma_{ij}\left(\mathbf{u}, e^p\right) n_j - \hat{t}_i\right] v_i^*\, dS = 0 \quad \forall\, \mathbf{u}^*, \mathbf{v}^* \tag{2.27}$$

$$\int_V \left[e^p - \ell^2\, \nabla^2 e^p - \bar{\varepsilon}^p\left(\mathbf{u}, e^p\right)\right] e^{p*}\, dV + \int_S e^p_{,i}\, n_i\, \gamma^*\, dS = 0 \quad \forall\, e^{p*}, \gamma^* \tag{2.28}$$

where $\mathbf{u}^* = \mathbf{0}$ on S_u and with $\boldsymbol{\sigma} = \boldsymbol{\sigma}\left(\mathbf{u}, e^p\right)$, as well as $\bar{\varepsilon}^p\left(\mathbf{u}, e^p\right)$ determined in VUMAT (ABAQUS EXPLICIT user defined material)

Now

$$\int_V \sigma_{ij,j}\, u_i^*\, dV = \int_V \left[\left(\sigma_{ij}\, u_i^*\right)_{,j} - \sigma_{ij}\, u_{i,j}^*\right] dV = \int_{S_t} \sigma_{ij}\, u_i^*\, n_j\, dS - \int_V \sigma_{ij}\, \varepsilon_{ij}^*\, dV \tag{2.29}$$

so 2.27 becomes

$$\int_V \left[-\sigma_{ij}\,\varepsilon^*_{ij} + \rho\, b_i\, u^*_i\right] dV + \int_{S_t} \left[\sigma_{ij}\, n_j\, (u^*_i + v^*_i) - \hat{t}_i\, v^*_i\right] dS = 0 \quad \forall\, \mathbf{u}^*, \mathbf{v}^* \tag{2.30}$$

Then we choose $\mathbf{v}^* = -\mathbf{u}^*$ and we end up with

$$\int_V \rho\, b_i\, u^*_i\, dV + \int_{S_t} \hat{t}_i\, u^*_i\, dS - \int_V \sigma_{ij}\,(\mathbf{u}, e^p)\, \varepsilon^*_{ij}\, dV = 0 \quad \forall\, \mathbf{u}^* \tag{2.31}$$

Additionally

$$-\int_V \ell^2\, \nabla^2 e^p\, e^{p*}\, dV = -\ell^2 \int_V e^p_{,ii}\, e^{p*}\, dV = -\ell^2 \int_V \left[\left(e^p_{,i}\, e^{p*}\right)_{,i} - e^p_{,i}\, e^{p\,*}_{,i}\right] dV = -\ell^2 \int_S e^p_{,i}\, e^{p*}\, n_i\, dS + \ell^2 \int_V e^p_{,i}\, e^{p\,*}_{,i}\, dV \tag{2.32}$$

and 2.28 becomes

$$\int_V \left\{\left[e^p - \bar{\varepsilon}^p\,(\mathbf{u}, e^p)\right] e^{p*} + \ell^2\, e^p_{,i}\, e^{p\,*}_{,i}\right\} dV + \int_S e^p_{,i}\left(\gamma^* - \ell^2\, e^{p*}\right) n_i\, dS = 0 \quad \forall\, e^{p*}, \gamma^* \tag{2.33}$$

Then we set $\gamma^* = \ell^2\, e^*$ to find

$$\int_V \left\{\left[e^p - \bar{\varepsilon}^p\,(\mathbf{u}, e^p)\right] e^{p*} + \ell^2\, e^p_{,i}\, e^{p\,*}_{,i}\right\} dV = 0 \quad \forall\, e^{p*} \tag{2.34}$$

Ultimately, we can express the residual for our gradient plasticity problem

$$R_1\,(\mathbf{u}, e^p) \equiv \int_V \rho\, b_i\, u^*_i\, dV + \int_{S_t} \hat{t}_i\, u^*_i\, dS - \int_V \sigma_{ij}\,(\mathbf{u}, e^p)\, \varepsilon^*_{ij}\, dV = 0 \quad \forall\, \mathbf{u}^*, e^{p*} \tag{2.35}$$

$$R_2\,(\mathbf{u}, e^p) \equiv \int_V \left\{\left[e^p - \bar{\varepsilon}^p\,(\mathbf{u}, e^p)\right] e^{p*} + \ell^2\, e^p_{,i}\, e^{p\,*}_{,i}\right\} dV = 0 \quad \forall\, \mathbf{u}^*, e^{p*} \tag{2.36}$$

Notice that $\boldsymbol{\sigma} = \boldsymbol{\sigma}\,(\mathbf{u}, e^p)$ as well as $\bar{\varepsilon}^p\,(\mathbf{u}, e^p)$ are determined in VUMAT

Generally, the user defined material subroutine operation can be defined as follows:

given $\boldsymbol{\sigma}_n$,$\mathbf{E}_n$,$\mathbf{E}^p_n$,$\bar{\varepsilon}^p_n$,e^p_n,$\boldsymbol{\Delta}\mathbf{E}$ and e^p_{n+1}

Calculate $\boldsymbol{\sigma}_{n+1}$,$\mathbf{E}^p_{n+1}$ and $\bar{\varepsilon}^p_{n+1}$.

Apparently, our VUMAT performs its calculations almost identically as the standard VUMAT, with the only difference being that σ_y is now a function of both $\bar{\varepsilon}^p$ as well as e^p.

2.1.4 Finite element implementation

The 8-node finite element used in the context of this thesis exhibits 32 degrees of freedom, thus for the following relations,consider $n = 32$

$$\underset{3\times 1}{\{u\,(\mathbf{x})\}} = \left\{\begin{array}{c} u_1\,(\mathbf{x}) \\ u_2\,(\mathbf{x}) \\ u_3\,(\mathbf{x}) \end{array}\right\}_{3\times 1} = \underset{3\times n}{[N_u\,(\mathbf{x})]}\,\underset{n\times 1}{\{d^e\}} \qquad \textit{and} \qquad \underset{3\times 1}{\{u^*\,(\mathbf{x})\}} = \underset{3\times n}{[N_u\,(\mathbf{x})]}\,\underset{n\times 1}{\{d^{e*}\}} \tag{2.37}$$

Node	DOF	Nodal unknowns
1	1-4	(u_1, u_2, u_3, e^p)
2	5-8	(u_1, u_2, u_3, e^p)
3	9-12	(u_1, u_2, u_3, e^p)
4	13-16	(u_1, u_2, u_3, e^p)
5	17-20	(u_1, u_2, u_3, e^p)
6	21-24	(u_1, u_2, u_3, e^p)
7	25-28	(u_1, u_2, u_3, e^p)
8	29-32	(u_1, u_2, u_3, e^p)

$$\underset{3\times n}{[N_u(\mathbf{x})]} = \left[\begin{array}{cccccccc} \underset{3\times4}{[N_{u1}]} & \underset{3\times4}{[N_{u2}]} & \underset{3\times4}{[N_{u3}]} & \underset{3\times4}{[N_{u4}]} & \underset{3\times4}{[N_{u5}]} & \underset{3\times4}{[N_{u6}]} & \underset{3\times4}{[N_{u7}]} & \underset{3\times4}{[N_{u8}]} \end{array} \right] \tag{2.38}$$

where

$$\underset{3\times4}{[N_{ui}]} = \left[\begin{array}{cccc} N_i & 0 & 0 & 0 \\ 0 & N_i & 0 & 0 \\ 0 & 0 & N_i & 0 \end{array} \right] \qquad i = 1, 2, ..., 8 \tag{2.39}$$

By operating accordingly, we end up with the following equations for the non-local plasticity e^p:

$$e^p(x) = \underset{1\times n}{\lfloor N_e(x) \rfloor} \underset{n\times1}{\{d^e\}} \qquad and \qquad e^{p*}(\mathbf{x}) = \underset{1\times n}{\lfloor N_e(\mathbf{x}) \rfloor} \underset{n\times1}{\{d^{e*}\}} \tag{2.40}$$

with

$$\underset{1\times n}{\lfloor N_e(x) \rfloor} = \left\lfloor \begin{array}{cccccccc} \underset{1\times4}{[N_{e1}]} & \underset{1\times4}{[N_{e2}]} & \underset{1\times4}{[N_{e3}]} & \underset{1\times4}{[N_{e4}]} & \underset{1\times4}{[N_{e5}]} & \underset{1\times4}{[N_{e6}]} & \underset{1\times4}{[N_{e7}]} & \underset{1\times4}{[N_{e8}]} \end{array} \right\rfloor \tag{2.41}$$

$$\underset{1\times4}{\lfloor N_{ei}(x) \rfloor} = \left\lfloor \begin{array}{cccc} 0 & 0 & 0 & N_i \end{array} \right\rfloor \quad i = 1, 2, ..., 8 \tag{2.42}$$

We can now formulate the element strain matrix as:

$$\underset{6\times1}{\{\varepsilon(\mathbf{x})\}} = \left\{ \begin{array}{c} \varepsilon_{11}(x) \\ \varepsilon_{22}(x) \\ \varepsilon_{33}(x) \\ 2\varepsilon_{12}(x) \\ 2\varepsilon_{13}(x) \\ 2\varepsilon_{23}(x) \end{array} \right\} = \underset{6\times n}{[B_u(\mathbf{x})]} \underset{n\times1}{\{d^e\}} \qquad \underset{6\times1}{\{\varepsilon^*(\mathbf{x})\}} = \underset{6\times n}{[B_u(\mathbf{x})]} \underset{n\times1}{\{d^{e*}\}} \tag{2.43}$$

We also write:

$$\underset{6\times n}{[B_u(\mathbf{x})]} = \left[\begin{array}{cccccccc} \underset{6\times4}{[B_{u1}]} & \underset{6\times4}{[B_{u2}]} & \underset{6\times4}{[B_{u3}]} & \underset{6\times4}{[B_{u4}]} & \underset{6\times4}{[B_{u5}]} & \underset{6\times4}{[B_{u6}]} & \underset{6\times4}{[B_{u7}]} & \underset{6\times4}{[B_{u8}]} \end{array} \right] \tag{2.44}$$

and note that:

$$\underset{6\times4}{[B_{ui}]} = \left[\begin{array}{cccc} \frac{\partial N_i}{\partial x} & 0 & 0 & 0 \\ 0 & \frac{\partial N_i}{\partial y} & 0 & 0 \\ 0 & 0 & \frac{\partial N_i}{\partial z} & 0 \\ \frac{\partial N_i}{\partial y} & \frac{\partial N_i}{\partial x} & 0 & 0 \\ \frac{\partial N_i}{\partial z} & 0 & \frac{\partial N_i}{\partial x} & 0 \\ 0 & \frac{\partial N_i}{\partial z} & \frac{\partial N_i}{\partial y} & 0 \end{array} \right] \qquad i = 1, 2, ..., 8 \tag{2.45}$$

For the derivatives of non local plastic deformation ∇e^p we express the following equations:

$$\underset{3\times1}{\{\nabla e^p(\mathbf{x})\}} = \left\{ \begin{array}{c} \frac{\partial e^p}{\partial x} \\ \frac{\partial e^p}{\partial y} \\ \frac{\partial e^p}{\partial z} \end{array} \right\}_{3\times1} = \underset{3\times n}{[B_e(\mathbf{x})]} \underset{n\times1}{\{d^e\}} \qquad and \qquad \underset{3\times1}{\{\nabla e^{p*}(\mathbf{x})\}} = \underset{3\times n}{[B_e(\mathbf{x})]} \underset{n\times1}{\{d^{e*}\}} \tag{2.46}$$

and finally

$$\underset{3\times n}{[B_e(\mathbf{x})]} = \left\lfloor \underset{3\times4}{[B_{e1}]} \quad \underset{3\times4}{[B_{e2}]} \quad \underset{3\times4}{[B_{e3}]} \quad \underset{3\times4}{[B_{e4}]} \quad \underset{3\times4}{[B_{e5}]} \quad \underset{3\times4}{[B_{e6}]} \quad \underset{3\times4}{[B_{e7}]} \quad \underset{3\times4}{[B_{e8}]} \right\rfloor \tag{2.47}$$

with

$$\underset{3\times4}{[B_{ei}]} = \begin{bmatrix} 0 & 0 & 0 & \frac{\partial N_i}{\partial x} \\ 0 & 0 & 0 & \frac{\partial N_i}{\partial y} \\ 0 & 0 & 0 & \frac{\partial N_i}{\partial z} \end{bmatrix} \qquad i = 1, 2, ..., 8 \tag{2.48}$$

At this stage recall from equation 2.36 that the residual of our problem can be defined as:

$$R \equiv \int_V \rho\, b_i\, u_i^*\, dV + \int_{S_t} \hat{t}_i\, u_i^*\, dS - \int_V \left[\sigma_{ij}\, \varepsilon_{ij}^* + (e^p - \bar{\varepsilon}^p)\, e^{p*} + \ell^2\, e^p_{,i}\, e^{p\,*}_{,i}\right] dV = 0 \quad \forall\, \mathbf{u}^*, e^{p*} \tag{2.49}$$

or in matrix form:

$$R = \underset{1\times N}{\lfloor D^* \rfloor} \underset{N\times1}{\{F\}} = 0 \quad \forall\, \underset{N\times1}{\{D^*\}} \qquad \underset{N\times1}{\{F\}} = \overset{\text{NELEM}}{\underset{e=1}{A}} \underset{n\times1}{\{f^e\}} \tag{2.50}$$

and ultimately,

$$\underset{n\times1}{\{f^e\}} = \int_{V^e} \underset{n\times3}{[N_u]^T} \underset{3\times1}{\{\rho\,\mathbf{b}\}}\, dV + \int_{S_t^e} \underset{n\times3}{[N_u]^T} \underset{3\times1}{\{\hat{t}\}}\, dS - \int_{V^e} \left[\underset{n\times6}{[B_u]^T} \underset{6\times1}{\{\sigma\}} + (e^p - \bar{\varepsilon}^p) \underset{n\times1}{\{N_e\}} + \ell^2 \underset{n\times3}{[B_e]^T} \underset{3\times1}{\{\nabla e^p\}} \right] dV\,. \tag{2.51}$$

2.1.5 Numerical integration of elastoplastic equations

Recall from section 2.1.2, that our VUMAT treats $\boldsymbol{\sigma}_n$,$\mathbf{E}_n$,$\mathbf{E}^p_n$,$\bar{\varepsilon}^p_n$,e^p_n,$\Delta\mathbf{E}$ and e^p_{n+1} as known quantities and eventually calculates $\boldsymbol{\sigma}_{n+1}$,$\mathbf{E}^p_{n+1}$ as well as $\bar{\varepsilon}^p_{n+1}$.

Also, note that the plastic predictor, as usual, is expressed as:

$$\boldsymbol{\sigma}^e = \boldsymbol{\sigma}_n + \mathbf{L}^e : \Delta\mathbf{E} \tag{2.52}$$

and, of course that, two possible conditions exist, regarding the yield criterion:

$$Condition \quad 1: \quad \Phi(\boldsymbol{\sigma}^e, \bar{\varepsilon}^p_n) \leq 0 \qquad which \quad refers \quad to \quad elastic \quad response \tag{2.53}$$

$$Condition \quad 2: \quad \Phi(\boldsymbol{\sigma}^e, \bar{\varepsilon}^p_n) > 0 \qquad which \quad refers \quad to \quad plastic \quad response \tag{2.54}$$

Acknowledge that for the above statements:

$$\boldsymbol{\sigma}_{n+1} = \boldsymbol{\sigma}^e, \qquad \bar{\varepsilon}^p_{n+1} = \bar{\varepsilon}^p_n \tag{2.55}$$

Then

$$\boldsymbol{\sigma}_{n+1}\left(\Delta\mathbf{E}^p\right)=\boldsymbol{\sigma}_n+\mathbf{L}^e:\left(\Delta\mathbf{E}-\Delta\mathbf{E}^p\right)=\boldsymbol{\sigma}^e-2\,G\,\Delta\mathbf{E}^p \qquad p_{n+1}=\sigma^e_{kk}=\text{known} \tag{2.56}$$

$$\mathbf{s}_{n+1}\left(\Delta\mathbf{E}^p\right)=\mathbf{s}^e-2\,G\,\Delta\mathbf{E}^p \tag{2.57}$$

$$\Delta\mathbf{E}^p=\Delta\lambda\,\mathbf{P}\left(\boldsymbol{\sigma}_{n+1}\right) \tag{2.58}$$

with 2.58, referring to the backward Euler equation

Now we express the following non-linear system of equations with $(\Delta\lambda,\Delta\mathbf{E}^p)$, as unknowns

$$\Phi\left(\boldsymbol{\sigma}_{n+1}\left(\Delta\mathbf{E}^p\right),\bar{\varepsilon}^p_{n+1}\left(\Delta\mathbf{E}^p\right)\right)=0 \tag{2.59}$$

$$\mathbf{F}\left(\Delta\lambda,\Delta\mathbf{E}^p\right)=\Delta\mathbf{E}^p-\Delta\lambda\,\mathbf{P}\left(\boldsymbol{\sigma}_{n+1}\left(\Delta\mathbf{E}^p\right)\right)=\mathbf{0} \tag{2.60}$$

where

$$\boldsymbol{\sigma}_{n+1}\left(\Delta\mathbf{E}^p\right)=\boldsymbol{\sigma}^e-2\,G\,\Delta\mathbf{E}^p \tag{2.61}$$

$$\bar{\varepsilon}^p_{n+1}\left(\Delta\mathbf{E}^p\right)=\bar{\varepsilon}^p_n+\sqrt{\frac{2}{3}\Delta\mathbf{E}^p:\Delta\mathbf{E}^p} \tag{2.62}$$

As a first estimate, for the initialization of the Newton loop, we can utilize the following:

$$\Delta\lambda=\frac{1}{\mathbf{L}_n}\mathbf{P}_n:\mathbf{L}^e:\Delta\mathbf{E}=\frac{2\,G}{\mathbf{L}_n}\mathbf{P}_n:\Delta\mathbf{E},\quad \mathbf{L}_n=\mathbf{P}_n:\mathbf{L}^e:\mathbf{P}_n+H_n=3\,G\,\bar{P}_n^2+H_n,\quad H_n=-\left.\frac{\partial\Phi}{\partial\bar{\varepsilon}^p}\right|_n\bar{P}_n \tag{2.63}$$

$$\Delta\mathbf{E}^p=\Delta\lambda\,\mathbf{P}_n \tag{2.64}$$

Ultimately and after $(\Delta\lambda,\Delta\mathbf{E}^p)$ become known quantities, we can calculate:

$$\boldsymbol{\sigma}_{n+1}=\boldsymbol{\sigma}^e-2\,G\,\Delta\mathbf{E}^p,\quad \Delta\bar{\varepsilon}^p=\sqrt{\frac{2}{3}\Delta\mathbf{E}^p:\Delta\mathbf{E}^p},\quad \bar{\varepsilon}^p_{n+1}=\bar{\varepsilon}^p_n+\Delta\bar{\varepsilon}^p,\quad \frac{\partial\Delta\bar{\varepsilon}^p}{\partial\Delta\bar{\varepsilon}^p}=\frac{2}{3\,\Delta\bar{\varepsilon}^p}\Delta\mathbf{E}^p \tag{2.65}$$

Without getting into deep detail, it can be proven that for our case, $(\boldsymbol{\sigma}^e,\boldsymbol{\sigma}_{n+1},\Delta\mathbf{E}^p)$ are all co-axial, thus the principal directions of $\Delta\mathbf{E}^p$ can be estimated from the principal directions of the elastic predictor such as:

$$\sigma^e=\sum_{i=1}^{3}\sigma^e_i\,\mathbf{n}^{(i)}\,\mathbf{n}^{(i)}=\text{known} \tag{2.66}$$

Of course, solving the system of equations 2.59 and 2.60 in the principal system defined by the principal directions $\mathbf{n}^{(i)}$ will significantly lessen the difficulty of our calculations. Obviously, at this point we have to express the following quantities with accordance to the principal system

$$\Delta\mathbf{E}^p=\sum_{i=1}^{3}\Delta E^p_i\,\mathbf{n}^{(i)}\,\mathbf{n}^{(i)},\quad \boldsymbol{\sigma}_{n+1}=\sum_{i=1}^{3}\sigma_i\,\mathbf{n}^{(i)}\,\mathbf{n}^{(i)},\quad \mathbf{P}_{n+1}=\sum_{i=1}^{3}P_i\,\mathbf{n}^{(i)}\,\mathbf{n}^{(i)} \tag{2.67}$$

where $\mathbf{n}^{(i)}$ are known

Notice that in a three dimensional problem and for the case of an arbitrary coordinate system, there are a total of 7 unknowns ($\Delta\lambda$ and the six elements of ΔE^p_{ij} matrix) while in the principal system, only 4 unknown

quantities exist $(\Delta\lambda, \Delta E_1^p, \Delta E_2^p, \Delta E_3^p)$. By re-writing equations 2.59, 2.60, 2.61 and 2.62 with respect to the principal system we get:

$$\Phi\left(\sigma_j\left(\Delta E_j^p\right), \bar{E}_{n+1}^p\left(\Delta E_j^p\right)\right) = 0 \tag{2.68}$$

$$F_i\left(\Delta\lambda, \Delta E_j^p\right) = \Delta E_i^p - \Delta\lambda\, P_i\left(\sigma_j\left(\Delta E_j^p\right), \bar{\varepsilon}^p\left(\Delta E_j^p\right)\right) = 0 \qquad (i = 1, 2, 3) \tag{2.69}$$

where

$$\sigma_i\left(\Delta E_i^p\right) = \sigma_i^e - 2\,G\,\Delta E_i^p \qquad (i = 1, 2, 3) \tag{2.70}$$

and

$$\bar{\varepsilon}_{n+1}^p\left(\Delta E_i^p\right) = \bar{\varepsilon}_n^p + \sqrt{\frac{2}{3}\left[\left(\Delta E_1^p\right)^2 + \left(\Delta E_2^p\right)^2 + \left(\Delta E_3^p\right)^2\right]} \tag{2.71}$$

Finally with the values of $\Delta\lambda$ as well as ΔE_i^p treated as known quantities we proceed with the following calculations

$$\Delta E^p = \sum_{i=1}^{3} \Delta E_i^p\, \mathbf{n}_i\, \mathbf{n}_i, \qquad \sigma_i = \sigma_i^e - 2\,G\,\Delta E_i^p, \qquad \sigma_{n+1} = \sum_{i=1}^{3} \sigma_i\, \mathbf{n}^{(i)}\, \mathbf{n}^{(i)} \tag{2.72}$$

$$\bar{\varepsilon}_{n+1}^p\left(\Delta E_j^p\right) = \bar{\varepsilon}_n^p + \sqrt{\frac{2}{3}\left[\left(\Delta E_1^p\right)^2 + \left(\Delta E_2^p\right)^2 + \left(\Delta E_3^p\right)^2\right]} \tag{2.73}$$

Where, in case the reader desires to obtain additional information concerning the derivatives in the principal direction regime, he should refer to Auricchio F. and Taylor R. L.

Prior to advancing to the next theoretical section, it becomes important to state that the gradient-enhanced elastoplasticity F.E. model presented in the context of the previous subsections corresponds to a more general finite element, which uses a total of 8 Gauss-Legendre integration points (full-integration scheme). For reasons comprehensively clarified in the following paragraphs, it is selected that our USER element employs a single integration point to execute every necessary numerical operation, thus it appears significant that the previously presented F.E. theory gets modified and generally upgraded.

2.2 Hourglass control with enhanced interpolation techniques

2.2.1 Reduced integration and Hourglass

For 3-D non-linear analysis, it is certainly common that a reduced integration scheme gets utilized for the purpose of performing the demanding integral operations which ultimately lead to an approximate solution for a given finite element problem. Of course, reduced integration not only significantly increases our model's computational efficiency, but at the same time it usually, successfully tackles the phenomenon of shear or volumetric locking by "underestimating" the finite element stiffness matrix (it is known that the finite element method "overestimates" the values of the element stiffness matrix, thus element locking could rise due to excessive stiffness which can be exhibited for particular loading and/or irregular geometries).

Unfortunately, apart from their beneficial effects mentioned above, reduced integration schemes can often cause hourglass, a "numerical anomaly" which gives rise to zero-energy modes and essentially occurs when an eigenvalue analysis performed on the element's stiffness matrix leads to an abnormal solution, where the number of calculated zero eigenvalues exceeds our elements' rigid body modes, as discussed above Figure 2.2. Definitely, these zero-energy modes are non-physical responses which produce meaningless results in the event they propagate through the computational mesh. Figure 2.1 demonstrates the deformation of an 8-node hexahedral element with a single integration point (at the center of the element) under bending moment. Notice that the vertical and horizontal dotted lines at the center of the element remain perpendicular preceding the application of the bending moment, which essentially proves that normal and shear stresses are indeed zero at the integration point and of course, that element deformation occurs with the absence of strain energy.

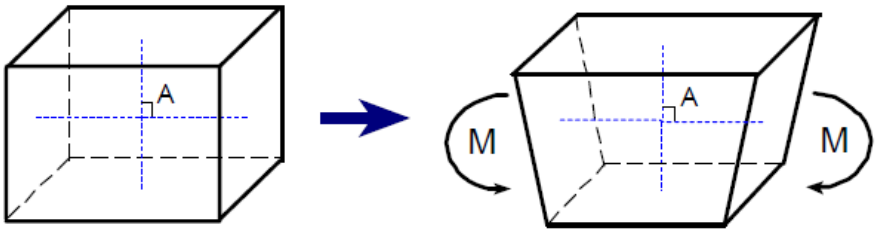

Figure 2.1: Shape change of a reduced integration element under bending moment, the "hourglass effect"

Figure 2.2 exhibits the fully-integrated/analytic stiffness matrix eigenvalues for a 4-node, 2-D finite element.Acknowledge that the actual F.E. deformation is expressed as a linear combination of the depicted modes. Also notice that 2 zero eigenvalues correspond to x and y axis translations and additionally that a zero eigenvalue refers to rotation around the z axis. In the event that a reduced integration scheme is introduced, the eigenproblem solution will lead to $\lambda_4 = \lambda_5 = 0$ because of the fact that the deformation values $(\varepsilon_x, \varepsilon_y, \gamma_{xy})$ are calculated as zero at the center of the element (position of the integration point). Thus spurious modes will rise and deformation will occur with zero deformation energy.

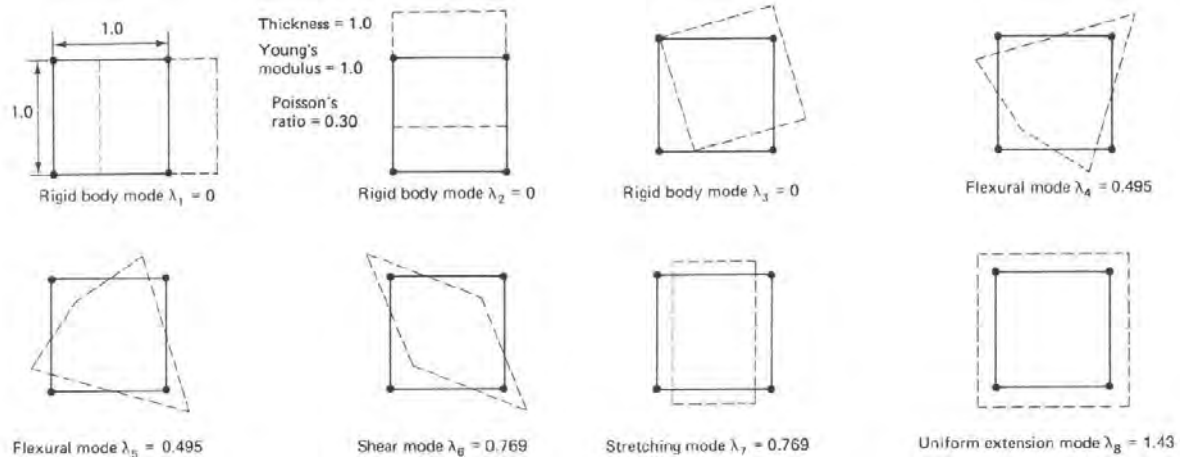

Figure 2.2: Analytic Stiffness matrix for the case of a 4-node,2-D finite element

2.2.2 Introduction to hourglass control

Assuredly, it is clearly understood that hourglass is a factor that typically leads to accuracy/analysis failure as well as an undesirable phenomenon that has to be methodically addressed and countered in order for a finite element simulation to be considered as successful.

However, prior to thoroughly discussing the specific hourglass control techniques implemented in our USER element, it is important to dedicate a few paragraphs in the direction of providing some general information/knowledge regarding hourglass control as well as finite element formulation and explicit/implicit algorithms.

For 3-D non-linear analysis, while high-order finite elements suffer from calculation difficulties concerning the Jacobian inversion of irregular geometries, low-order elements and especially the eight-node hexahedral element is characterized by exceptional computational efficiency , robustness and ease of use. Thus, for plastic, elastoplastic, hyperelastic and for non-linear materials in general, various formulations have been developed for the sake of enhancing and eventually maximizing the efficiency of the eight-node brick. Of course the implicit algorithms tend to be more accurate, however they present inadequate computational efficiency and consequently reduced integration schemes (for the case of the hexahedral, a single point Gauss-Legendre integration is performed) are commonly implemented in finite element analysis.

Unfortunately, for certain demanding mesh types (excessively deformed) or for extreme non-linear conditions and quasi-static analysis, the convergence rate is so strongly unsatisfying (even for reduced integrated elements) that it becomes obligatory to sacrifice the reduced error of implicit algorithms for the improved convergence of explicit formulation. With all the above being said, an explicit formulation for hourglass control on non-linear elements is presented during the last segment of this theoretical subsection.

As far as it concerns the elimination of spurious modes on reduced integrated and non-linear, finite elements , a lot of papers including those of Liu W. K. , Ong J. S. and Uras R. A., Koh B. C. and Kikuchi N., Zhu Y. Y. and Cescotto S. as well as Belytschko T. and Binderman L. P. suggest different methods in the direction of resolving the issue of hourglass. The specific USER element presented and tested through a series of patch tests in the context of this Thesis, takes advantage of an hourglass control theory which combines the incompatible modes method with the physical stabilization method. This theory features enhanced strain fields which do not require any matrix inversions to solve for the internal element degrees of freedom, it was primarly introduced by Puso M. A. and afterwards slightly modified as well as upgraded prior to getting integrated in our USER finite element.

Definitely, an in-depth presentation of the enhanced interpolation hourglass control theory does not comply with the overall purpose of this specific thesis, thus it appears more appropriate that a brief discussion regarding the model is pursued, so as the reader gets to understand the general concept and equations implemented in the hexahedral finite element formulation. After all, in the event that an extensive comprehension of the enhanced interpolation theory is desired the user should refer to the papers and books noted in the Bibliographic section. Ultimately, during the last segment of this subsection, a demonstration of the incremental formulation for our User element in explicit finite element setting, is performed.

2.2.3 Presentation of the enhanced assumed strain hourglass control model

The "Assumed strain" method assumes geometric linearity and treats stresses $\boldsymbol{\sigma}^h$,displacement increments $\Delta\mathbf{u}^h$ as well as displacement gradients $\Delta\mathbf{L}^h$ as independent unknowns. Note that subscript h will be deployed if necessary to declare the interpolated field. Also recall from theoretical section 2.1, that our gradient plasticity model introduces an additional nodal unknown (non local plastic deformation), thus the element formulation presented below, also includes e^p as well g_i, q_i (where g_i and q_i are introduced due to mixed formulation) to the set of primary unknowns. Recall also, from N. Aravas and J. Papadioti that:

$$e^p + q_{i,i} = \bar{\varepsilon}^p \tag{2.74}$$

$$g_i = e^p{}_{,i} \tag{2.75}$$

$$q_i = -\ell^2\, g_i \tag{2.76}$$

Prior to proceeding to the theoretical discussion, it is important to state that the reader should consult appendinx A for additional information regarding the matrices involved in this section.

For openers, the variational statements can be expressed as:

$$\int_\Omega \left(\sigma^h_{ij,j} + \rho\, b_i - \rho\, \ddot{u}^h_i\right) \delta u^h_i \, d\Omega + \int_{\partial\Omega_t} \left(\hat{t}_i - \sigma^h_{ij}\, n_j\right) \delta u_i \, d\Omega + \int_\Omega \left[\sigma^h_{ij} - \sigma_{ij}\left(\Delta\mathbf{L}^h\right)\right] \delta L_{ij} \, d\Omega + \\ + \int_\Omega \left(\Delta L^h_{ij} - \Delta u^h_{i,j}\right) \delta\sigma_{ij} \, d\Omega = 0 \forall\ \delta\mathbf{u},\ \delta\mathbf{L},\ \delta\boldsymbol{\sigma}\,. \tag{2.77}$$

$$\int_V \left(e^p + q_{i,i} - \bar{\varepsilon}^p\right) e^p{*}\, dV + \int_S -\frac{q_i}{\ell^2} n_i\, \gamma^*\, dS = 0 \quad \forall\, e^p{*}, \gamma^* \tag{2.78}$$

$$\int_V \left(g_i - e^p{}_{,i}\right) q^*_i \, dV = 0 \quad \forall\, q^*_i \tag{2.79}$$

$$\int_V \left(q_i + \ell^2\, g_i\right) g^*_i \, dV = 0 \quad \forall\, g^*_i \tag{2.80}$$

While the element interpolation for the u_i primary unknowns is defined in the equations below

$$\underset{3\times1}{\left\{\Delta u^h\left(\mathbf{x}\right)\right\}}=\underset{3\times24}{\left[N\left(\mathbf{x}\right)\right]}\underset{24\times1}{\left\{\Delta u_e^N\right\}}\Rightarrow\underset{9\times1}{\left\{\nabla\left(\Delta u^h\right)\left(\mathbf{x}\right)\right\}}=\underset{9\times1}{\left\{\Delta u_{i,j}^h\left(\mathbf{x}\right)\right\}}=\underset{9\times24}{\left[B_L\left(\mathbf{x}\right)\right]}\underset{24\times1}{\left\{\Delta u_e^N\right\}} \tag{2.81}$$

$$\underset{9\times1}{\left\{\Delta L^h\left(\mathbf{x}\right)\right\}}=\left(\underset{9\times24}{\overline{\left[B_L\right]}}+\underset{9\times24}{\left[B_{\text{stab}}\left(\mathbf{x}\right)\right]}\right)\underset{24\times1}{\left\{\Delta u_e^N\right\}}+\underset{9\times6}{\left[G\left(\mathbf{x}\right)\right]}\underset{6\times1}{\left\{\Delta\alpha_e^N\right\}} \tag{2.82}$$

$$\underset{9\times1}{\left\{\sigma^h\left(\mathbf{x}\right)\right\}}=\underset{9\times1}{\left\{\sigma_0\right\}}=\text{const.} \tag{2.83}$$

Where

$$\underset{9\times24}{\overline{\left[B_L\right]}}=\frac{1}{V^e}\int_{\Omega^e}\underset{9\times24}{\left[B_L\left(\mathbf{x}\right)\right]}d\Omega \tag{2.84}$$

and we choose $\underset{9\times24}{\left[B_{\text{stab}}\left(\mathbf{x}\right)\right]}$ as well as $\underset{6\times6}{\left[G\left(\mathbf{x}\right)\right]}$ so that

$$\underset{9\times24}{\left[B_{\text{stab}}|_{\xi=\mathbf{0}}\right]}=\underset{9\times24}{\left[\mathbf{0}\right]},\underset{9\times24}{\left[G|_{\xi=\mathbf{0}}\right]}=\underset{9\times6}{\left[\mathbf{0}\right]} \tag{2.85}$$

$$\int_{\Omega^e}\underset{9\times24}{\left[B_{\text{stab}}\left(\mathbf{x}\right)\right]}d\Omega=\underset{9\times24}{\left[\mathbf{0}\right]},\int_{\Omega^e}\underset{9\times24}{\left[G\left(\mathbf{x}\right)\right]}d\Omega=\underset{9\times6}{\left[\mathbf{0}\right]} \tag{2.86}$$

Notice that 2.82 introduces $\underset{6x1}{\left\{\Delta\alpha_e^N\right\}}$, however these additional 6 degrees of freedom are internal instead of nodal and eventually they are eliminated by static condensation. As Puso M. A. states, $\underset{6x1}{\left\{\Delta\alpha_e^N\right\}}$ is implemented in the finite element formulation in the direction of addressing the phenomenon of shear locking. Afterwards we can express the element interpolation for e^p as:

$$e^p\left(\mathbf{x}\right)=\underset{1\times8}{\left\lfloor N_{e^p}\left(\mathbf{x}\right)\right\rfloor}\underset{8\times1}{\left\{e_e^{pN}\right\}}\qquad e^{p*}\left(\mathbf{x}\right)=\underset{1\times8}{\left\lfloor N_{e^p}\left(\mathbf{x}\right)\right\rfloor}\underset{8\times1}{\left\{e_e^{pN}\right\}} \tag{2.87}$$

$$\underset{3\times1}{\left\{\nabla e^p\left(\mathbf{x}\right)\right\}}=\underset{3\times8}{\left[B_{e^p}\left(\mathbf{x}\right)\right]}\underset{8\times1}{\left\{e_e^{pN}\right\}}\qquad\underset{3\times1}{\left\{\nabla e^{p*}\left(\mathbf{x}\right)\right\}}=\underset{3\times8}{\left[B_{e^p}\left(\mathbf{x}\right)\right]}\underset{8\times1}{\left\{e_e^{pN*}\right\}} \tag{2.88}$$

$$\underset{3\times1}{\left\{g\left(\mathbf{x}\right)\right\}}=\left(\underset{3\times8}{\overline{\left[B_{e^p}\right]}}+\underset{3\times8}{\left[B_{e^p}^{\text{stab}}\left(\mathbf{x}\right)\right]}\right)\underset{8\times1}{\left\{e_e^{pN}\right\}}\qquad\underset{3\times1}{\left\{g^*\left(\mathbf{x}\right)\right\}}=\left(\underset{3\times8}{\overline{\left[B_{e^p}\right]}}+\underset{3\times8}{\left[B_{e^p}^{\text{stab}}\left(\mathbf{x}\right)\right]}\right)\underset{8\times1}{\left\{e_e^{pN*}\right\}} \tag{2.89}$$

$$\underset{3\times1}{\left\{q\left(\mathbf{x}\right)\right\}}=\underset{3\times1}{\left\{q_0\right\}}\qquad\underset{3\times1}{\left\{q^*\left(\mathbf{x}\right)\right\}}=\underset{3\times1}{\left\{q_0^*\right\}} \tag{2.90}$$

with

$$\underset{3\times8}{\left[B_{e^p}^{\text{stab}}|_{\xi=\mathbf{0}}\right]}=\underset{3\times8}{\left[\mathbf{0}\right]},\qquad\int_{\Omega^e}\underset{3\times8}{\left[B_{e^p}^{\text{stab}}\left(\mathbf{x}\right)\right]}d\Omega=\underset{3\times8}{\left[\mathbf{0}\right]} \tag{2.91}$$

At this stage recall that the shape functions can be written in the following form:

$$\underset{8\times1}{\left\{N\left(\mathbf{x}\right)\right\}}=\underset{8\times1}{\left\{b_0\right\}}+\sum_{j=1}^{3}\underset{8\times1}{\left\{b_j\right\}}x_j+\sum_{k=1}^{4}h_k\left(\xi\left(\mathbf{x}\right)\right)\underset{8\times1}{\left\{\gamma_k\right\}} \tag{2.92}$$

with

$$\underset{8\times1}{\left\{b_0\right\}}+\sum_{j=1}^{3}\underset{8\times1}{\left\{b_j\right\}}x_j \tag{2.93}$$

resulting to constant strain, i.e. $\mathbf{B}$ matrix and

$$\sum_{k=1}^{4}h_k\left(\xi\left(\mathbf{x}\right)\right)\underset{8\times1}{\left\{\gamma_k\right\}} \tag{2.94}$$

leading to non-constant strain and exploited for stabilization purposes.

Of course $\underset{8\times1}{\{x_i\}}$, $(i=1,2,3)$ represent the nodal Cartesian coordinates. Also

$$\underset{8\times1}{\{\gamma_i\}} = \frac{1}{8}\left[\underset{8\times1}{\{h_i\}} - \sum_{j=1}^{3}\left(\underset{1\times8}{\lfloor h_i \rfloor}\ \underset{8\times1}{\{x_j\}}\right)\underset{8\times1}{\{b_j\}}\right] \qquad (i=1,2,3,4) \tag{2.95}$$

$$\underset{8\times1}{\{b_i\}} = \frac{1}{8}\sum_{j=1}^{3}\left(J_0^{-1}\right)_{ji}\underset{8\times1}{\{\xi_j\}} = \left(\frac{\partial}{\partial x_i}\underset{8\times1}{\{N\}}\right)_{\xi=\mathbf{0}} \qquad (i=1,2,3) \tag{2.96}$$

At this moment, we can express the residuals as:

$$R \equiv \int_{\Omega}\rho\, b_i\,\delta u_i\, d\Omega + \int_{\partial\Omega_t}\hat{t}_i\,\delta u_i\, d\Omega - \int_{\Omega}\sigma_{ij}\left(\Delta\mathbf{L}^h\right)\delta L_{ij}\, d\Omega - \int_{\Omega}\rho\,\ddot{u}_i\,\delta u_i\, d\Omega = 0 \forall\ \delta\mathbf{u},\ \delta\mathbf{L} \tag{2.97}$$

ultimately we get

$$\underset{N\times1}{\{R_u\}} \equiv \underset{N\times1}{\left\{F^{ext}\right\}} - \overset{\text{NELEM}}{\underset{e=1}{\text{A}}}\underbrace{\int_{d\Omega}\left(\underset{24\times9}{\left[\overline{B_L}\right]^T} + \underset{24\times9}{\left[B_{\text{stab}}\left(\xi\right)\right]^T}\right)\underset{9\times1}{\left\{\boldsymbol{\sigma}\left(\Delta\mathbf{L}^h\left(\xi\right)\right)\right\}}\, d\Omega}_{\underset{24\times1}{\{\mathbf{f}_u^e\}}} - \underset{N\times N}{[M]}\ \underset{N\times1}{\left\{\ddot{\mathbf{u}}^N\right\}} = \{\mathbf{0}\} \tag{2.98}$$

where

$$\underset{9\times24}{\left[B_{\text{stab}}\left(\xi\right)\right]} = \frac{J_0}{J\left(\xi\right)}\underset{9\times9}{\left[K_0\right]}\underset{9\times24}{\left[\tilde{B}_{\text{stab}}\left(\xi\right)\right]}\underset{24\times24}{\left[G\right]} \tag{2.99}$$

$$\underset{9\times24}{\left[\tilde{B}_{\text{stab}}\left(\xi\right)\right]} = \sum_{i=1}^{4}\underset{9\times3}{\left[\hat{B}_i\left(\xi\right)\right]}\underset{3\times24}{\left[\Gamma_i\right]^T} \tag{2.100}$$

and we can calculate $\underset{6\times1}{\left\{\Delta\alpha_e^N\right\}}$ from the equations below

$$\int_{d\Omega}\underset{6\times9}{\left[G\left(\xi\right)\right]^T}\underset{9\times1}{\left\{\boldsymbol{\sigma}\left(\Delta\mathbf{L}^h\left(\xi\right)\right)\right\}}\, d\Omega = \underset{6\times1}{\{\mathbf{0}\}} \tag{2.101}$$

$$\int_{d\Omega}\underset{6\times9}{\left[G\left(\xi\right)\right]^T}\underset{9\times1}{\left\{\boldsymbol{\sigma}\left(\Delta\mathbf{L}^h\left(\xi\right)\right)\right\}}\, d\Omega = \underset{6\times1}{\{\mathbf{0}\}} \Rightarrow \underset{6\times1}{\left\{\Delta\alpha^N\right\}} = -\underset{6\times6}{\left[K_{\alpha\alpha}\right]^{-1}}\underset{6\times24}{\left[K_{\alpha u}\right]}\underset{24\times1}{\left\{\Delta u^N\right\}} \tag{2.102}$$

Note that

$$\underset{9\times6}{\left[G\left(\xi\right)\right]} = \frac{J_0}{J\left(\xi\right)}\underset{9\times9}{\left[K_0\right]}\underset{9\times6}{\left[\tilde{G}\left(\xi\right)\right]} \tag{2.103}$$

Without getting into deep detail, we can now express the equations for the external forces stabilization vectors. It can be proven that for the u_i primary unknowns we can write:

$$\underset{24\times1}{\{f_{\text{stab}}^e\}} = J_0\sum_{i=1}^{4}\underset{24\times3}{\left[M_i\right]^T}\underset{3\times1}{\left\{f_i\right\}} \tag{2.104}$$

with

$$\underset{3\times1}{\{f_i\}} = \int_{d\Omega}\underset{3\times9}{\left[\hat{B}_i\right]^T}\underset{9\times9}{\left[K_0\right]^T}\underset{9\times1}{\left\{\sigma_{\text{stab}}\right\}}\, d\Omega, \quad \underset{24\times3}{\left[M_i\right]^T} = \underset{24\times3}{\left[\Gamma_i\right]}\underset{3\times3}{\left[J_0\right]} \tag{2.105}$$

and finally we end up with the stabilization equation:

$$\underset{3\times1}{\{f_i\}} \cong \underset{3\times1}{\{f_i\}_n} + \underset{3\times1}{\{\Delta f_i\}} \tag{2.106}$$

where

$$\underset{3\times1}{\{\Delta f_i\}} = \underset{3\times24}{\left[K^i_{uu}\right]} \underset{24\times1}{\left\{\Delta u^N_e\right\}} + \underset{3\times6}{\left[K^i_{\alpha u}\right]^T} \underset{6\times1}{\left\{\Delta \alpha^N_e\right\}} \tag{2.107}$$

$$\underset{3\times3}{\left[K^{ij}_{uu}\right]} = \int_{d\Omega} \underset{3\times9}{\left[\hat{B}_i\right]^T} \underset{9\times9}{\left[\tilde{C}_0\right]} \underset{9\times3}{\left[\hat{B}_j\right]} d\Omega \qquad i,j = 1,2,3,4 \tag{2.108}$$

$$\underset{3\times24}{\left[K^i_{uu}\right]} = \sum_{j=1}^{4} \underset{3\times3}{\left[K^{ij}_{uu}\right]} \underset{3\times24}{\left[M_j\right]} \quad \underset{3\times24}{\left[M_i\right]} = \underset{3\times3}{\left[J_0\right]^T} \underset{24\times3}{\left[\Gamma_i\right]^T} \qquad i = 1,2,3,4 \tag{2.109}$$

By operating accordingly we can obtain the following relation for e^p:

$$\underset{8\times1}{\{r^e_{e^p}\}} = 8J_0\left(\bar{\varepsilon}^p_0 - e^p{}_0\right) \underset{1\times8}{\{N_{e^p}\}}_{\xi=\mathbf{0}} - \left(\ell^2 V_e \underset{8\times3}{\overline{[B_{e^p}]}^T} \underset{3\times8}{\overline{[B_{e^p}]}} + \ell^2 \int_{d\Omega} \underset{8\times3}{\left[B^{\text{stab}}_{e^p}(\xi)\right]^T} \underset{3\times8}{\left[B^{\text{stab}}_{e^p}(\xi)\right]} d\Omega \right) \underset{8\times1}{\left\{e^p{}^N_e\right\}} = \underset{8\times1}{\{0\}} \tag{2.110}$$

and later we end up with

$$\underset{N\times1}{\{R_u\}} \equiv \overset{NELEM}{\underset{e=1}{A}} \underset{8\times1}{\{r^e_{e^p}\}} = \underset{N\times1}{\{0\}} \tag{2.111}$$

Of course for the ($\mathbf{u}$+e^p) formulation, we must combine the residual equations for the u_i primary unknowns with those of e^p and obtain the full residual vector: $\underset{32\times1}{\{R^e\}}$ and the full residual matrix is assembled in accordance with the following "rules":

$$\left(r^e_{e^p}\right)_i \rightarrow R^e_{4i} \qquad i = 1,2,K,8 \tag{2.112}$$

$$\left(J^e_{\text{equil},e^p}\right)_{3(i-1)+k,j} \rightarrow J^e_{4(i-1)+k,4j} \qquad i = 1,2,K,8 \quad k = 1,2,3 \tag{2.113}$$

Applications section

The accuracy of the elements is arguably the most important contributor to a successful finite element analysis. Thus, it is necessary that every newly proposed finite element is subjected to a series of demanding patch tests in order for the designer to verify that their performance is satisfactory prior to their actual use in any application.

It became evident that a comprehensive set of element test problems which takes into consideration various parameters that affect the element accuracy, such as the type of loading, the element geometry, the material properties or the plasticity flow rule, had to be designed. Of course, the above mentioned patch test series had to also be able to "detect" the most critical indicators of element accuracy failure: the zero energy-modes and the volumetric as well as shear locking phenomena.

It is believed that a finite element that does not pass a series of challenging tests, should not even be used for commercial or research purposes, however it is more than critical for the user to understand that even if the element successfully corresponds to the needs of a certain problem set, it is not assured that its performance is sufficient since the rate of convergence could possibly be observably slow for any practical use.

In the context of this thesis' applications section, a variety of tests is utilized in the direction of validating the suitability of the enhanced assumed strain method for hourglass control on hexahedral, non-linear finite elements. In general, straight cantilever beams dominate this particular problem set, due to their evident simplicity and because of the fact that every principal element deformation mode can be evoked by loads applied to their free end. Ultimately, it is indeed important to state that every patch test is also executed using the ABAQUS elements: C3D8, C3D8H and C3D8R and of course comparison of the results is performed not only among the ABAQUS elements and the USER element but also between every element and the analytic (benchmark) solution. Note that when applicable, the analysis for ABAQUS elements is run implicitly so as to achieve simulation results with increased accuracy.

Prior to advancing to our first application, it is important to state that β is a parameter which controls the "amount of information" actually used in finite element stiffness matrix calculations. Our subroutine provides the user with the option of manually setting β equal to zero and thus neglecting certain elements of $[K_{uu}]$(matrices involved in the calculation of hourglass stabilization forces - Refer to N. Aravas and J. Papadioti), or else retaining the β parameter value equal to 1 and performing every necessary numerical operation while using the complete $[K_{uu}]$ matrices. Puso M. A. mentions that we can set β =0 to eliminate shear locking in rectangular parallelepiped elements with sides parallel to the coordinate axes, but of course the user can choose any value for β parameter that ranges from zero to one in the direction of "adjusting" the USER element to the needs of any given problem/geometry in his attempt of tackling the phenomenon of shear locking.

3.1 Patch test 1: Extension of a 3-D, 7-element model

Apparently, geometrical deviation from the element's standard shape (in the case of the hexahedral finite element the standard shape is a cube) can lead to accuracy failure, especially when the numerical analysis transits from the purely elastic to the non-linear region or in the instance of demanding loading conditions. Taking all the above into consideration, it becomes evident that our USER element has to be tested with a mesh of sensibly irregular finite elements and of course, it is understood that the problem proposed by Macneal R. H. and Harder R. L., perfectly fits the needs of our study. Our geometry consists of a unit, solid cube, the selected material properties are: E=$2 * 10^5 MPa$; ν=0.25 ; $\sigma_0 = 400MPa$ and a displacement of magnitude 0.4 mm is implemented in the top face of the cube. Figure 3.1 depicts this particular patch test's geometry and provides additional information regarding the exact position of nodes in the mesh.

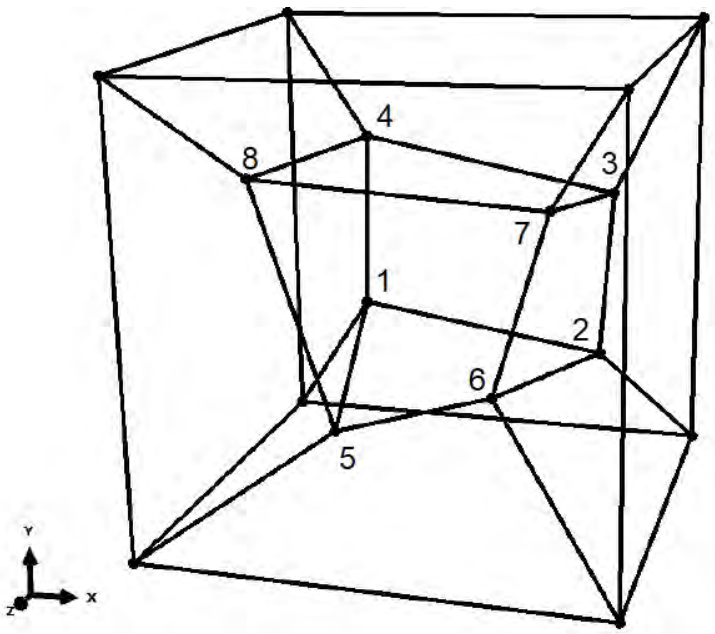

	X	X	Z
1	0.249	0.342	0.192
2	0.826	0.288	0.288
3	0.85	0.649	0.263
4	0.273	0.75	0.23
5	0.32	0.186	0.643
6	0.677	0.305	0.683
7	0.788	0.693	0.644
8	0.165	0.745	0.702

Figure 3.1: Patch test number one, geometry description. Length Units: mm

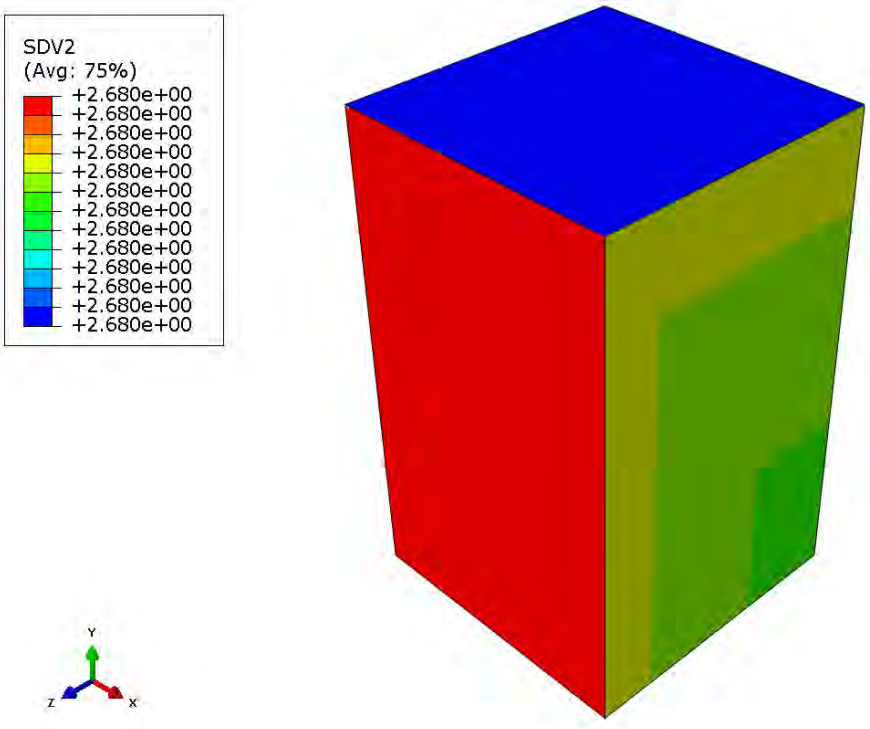

Figure 3.2: σ_{yy} principal stress posterior to the implementation of the displacement

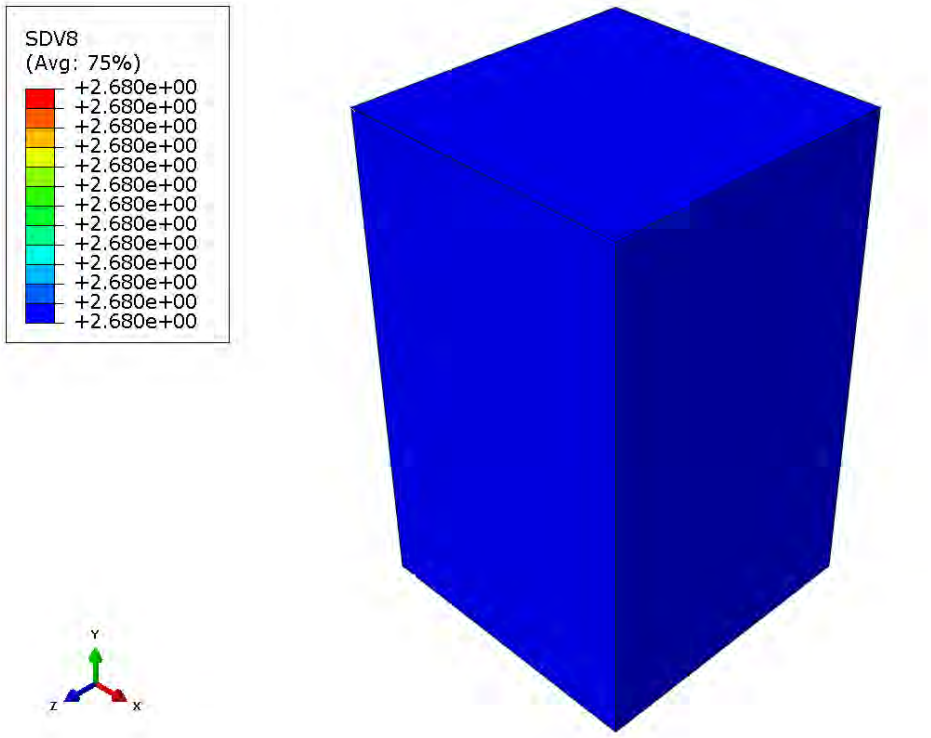

Figure 3.3: Equivalent Von Misses stress σ_e at the end of the analysis

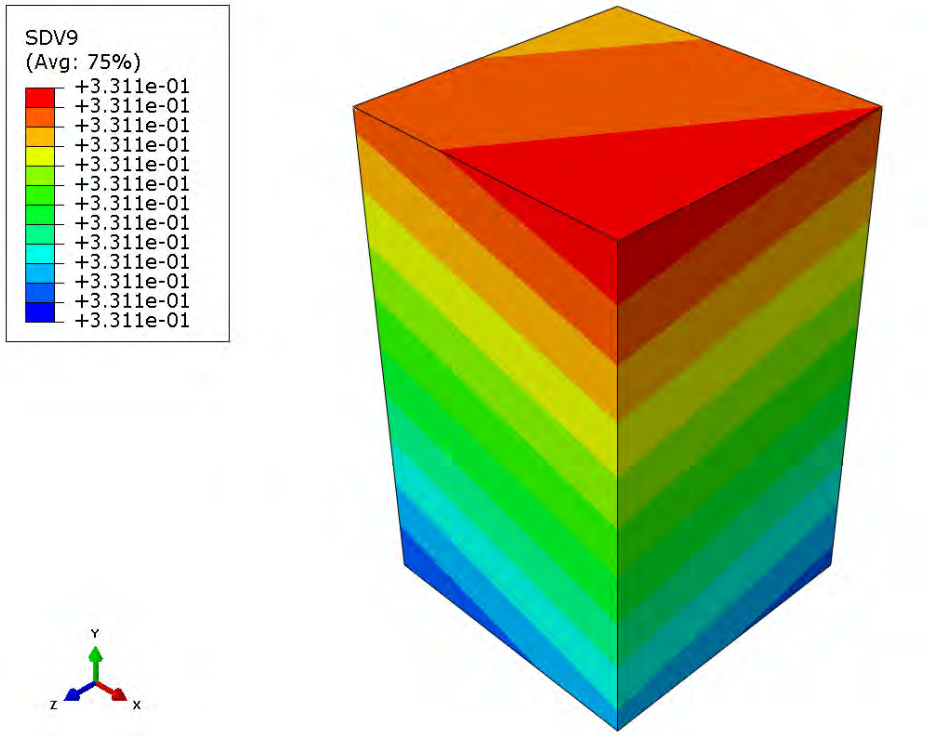

Figure 3.4: Results for equivalent plastic strain e_p

Obviously this analysis' results confirm that the principal stress at the direction of the implemented displacement, the equivalent stress as well as the plastic deformation, are indeed homogenous even during the last increments of the explicit analysis where our material exhibits nonlinear behavior. Undoubtedly this is an indication that our USER element has the ability to provide trustworthy results for the case of unidirectional extension, without displaying any signs of accuracy failure.

3.2 Patch test 2: Nearly incompressible eigenvalue test

In the direction of testing our element's behavior in the nearly incompressible range, an eigenvalue analysis is performed for the stiffness matrix of a cubic element with sides of *length* =1 m. While Young's modulus remains constant at E=1 GPa, two separate tests are executed in the elastic material regime and for different values of Poisson's constant (ν=0.3 and ν=0.499). Note that, as it is not possible to perform an eigenvalue analysis using the ABAQUS explicit solver (explicit solution does not formulate an element stiffness matrix), our analysis is based on the ABAQUS implicit solver. Of course, in the context of this particular patch problem, a variety of USER elements (UEL/UMAT) with or without hourglass control are tested and the results of the eigenvalue problem are presented and discussed in the paragraphs below.

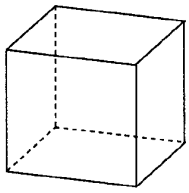

Figure 3.5: A simple unit cube used for our eigenvalue analysis

	ν=0.3			ν=0.499	
Full-integration	1 int. Point/ No hourglass control	1 int. Point/ Hourglass Control	Full-integration	1 int. Point/ No hourglass control	1 int. Point/ Hourglass Control
2.0436833	2.0006006	1.2506665	250000.25	250000.1	2500.001
2.0436833	2.0006	2.0013997	2.0436667	2.0010003	2.0009998
2.0384875	1.9980023	1.9988005	2.0436667	2.001	1.9980019
1.3485611	1.2498341	1.3346667	2.0376727	1.998002	1.3326688
1.3468292	0.38473083	1.3329347	1.3485556	0.33350025	1.3346667
1.3468292	0.38473083	2.0013997	1.3465576	0.33350025	2.0009998
1.250501	0.38448105	0.66675602	1.3465576	0.33325042	0.66666738
0.6713875	0.38448099	1.3329347	0.67129696	0.33325039	1.3326688
0.385	0.38439754	0.25644456	0.33366688	0.33316696	0.38904827
0.385	0.12504999	0.3842182	0.33366688	0.125	0.2222372
0.38425011	1.86005E-15	0.30233347	0.33291706	8.82846E-12	0.38871577
0.38425011	1.63917E-15	0.38488457	0.33291706	4.85823E-12	0.38871577
0.38400037	1.34838E-15	0.38488457	0.33266738	3.89441E-12	0.055448319
0.25633346	1.1027E-15	0.38438459	0.22211142	3.89441E-12	0.055670393
0.19241663	9.88082E-16	0.30219119	0.16675007	2.90566E-12	0.33285576
0.19220889	5.22924E-16	0.38438459	0.16654244	2.14339E-12	0.33352205
0.19220889	3.30391E-16	0.30219119	0.16654244	2.14339E-12	0.33352205
0.12504999	2.82838E-16	0.064000133	0.125	9.40638E-13	0.33302221
0.10683768	2.82838E-16	0.064222242	0.092578451	9.40638E-13	0.33302221
0.10683768	1.44028E-17	0.19233347	0.092578451	1.02902E-15	0.16667796
0.10682401	-2.1861E-16	0.12504999	0.092564815	8.41221E-16	0.16667758
0.071262329	-2.1861E-16	0.192333	0.061756196	2.99024E-16	0.16667758
0.071262329	-3.07875E-16	0.192333	0.061756196	-5.29225E-16	0.12500003
0.071142059	-4.75713E-16	0.07121611	0.061635951	-2.32721E-13	0.061769502
0.064249753	-6.12486E-16	0.07121611	0.055694194	-9.31093E-13	0.061714076
0.064083292	-7.21507E-16	0.071271547	0.055527777	-9.31093E-13	0.061714076
0.000249638	-8.56278E-16	0.000249725	0.000249575	-2.12492E-12	0.000249782
0.000249638	-1.02653E-15	0.000249725	0.000249575	-2.5458E-12	0.000249782
1.70295E-14	-1.2221E-15	2.8157E-11	1.17679E-08	-2.5458E-12	1.56383E-07
1.09565E-15	-1.2558E-15	8.52286E-16	2.89295E-12	-4.18102E-12	-1.30261E-16
9.01171E-16	-1.61703E-15	1.01666E-15	-1.79229E-12	-5.1151E-12	-6.69596E-15
-1.05855E-15	-1.68363E-15	5.6315E-17	-2.52216E-12	-1.34743E-11	-6.69596E-15

Figure 3.6: Eigenvalue analysis results for ν=0.3 and ν=0.499

Our model presents a total of 32 degrees of freedom (8 nodes with u_1,u_2,u_3 and e^p treated as unknows for each node), thus the overall number of eigenvalues for this problem is, as well 32, and it is expected that the eigenproblem solution leads to exactly 6 zero eigenvalues (for this 3-D problem there are 6 acceptable rigid body motions, 3 translational and 3 rotational). Of course, when ν=0.499 the correct eigenproblem solution should also include an infinite eigenvalue which corresponds to an incompressible mode. As anticipated, the 8-node fully integrated element (utilizing a 2x2x2 Gauss-Legendre integration scheme) performs perfectly for both given values of Poisson's ratio, however when it comes to the case of the reduced integrated element with no hourglass control, more than 6 zero eigenvalues are observed. Obviously, from a total of 32 eigenvalues, only 10 are non-zero which essentially means that our solution consists of 16 zero-energy modes (spurious mechanisms with no physical meaning) and that accuracy failure has occurred.

With all that being said it is understandable that every reduced integrated finite element formulation has to take into consideration an hourglass control theory. Eventually, this eigenvalue analysis proves that the only hexahedral that produces meaningful results is the finite element which employs the enhanced assumed strain hourglass control model discussed in the context of section 2.2.

3.3 Patch test 3: Two-element beam in pure bending

Test number 3 introduces a two-element, elastic cantilever beam which is subjected to pure bending. The vertical tip displacement u_2 is measured for different values of the applied skew distance "a" and this patch problem aims to evaluate the distortion sensitivity of the USER element, thus a variety of irregularly shaped element meshes is examined and ultimately the analysis results are compared with the benchmark solution. Our cantilever beam is of length=10 mm; height=2 mm; thickness=1 mm and the elastic material properties are set: E=3000 MPa; ν=0. As displayed in figure Figure 3.7a, a force couple is applied at our geometry's tip and the implement force is of magnitude F=$10^{-3}N$ in the direction of generating an equivalent bending moment M=0.002 Nmm.

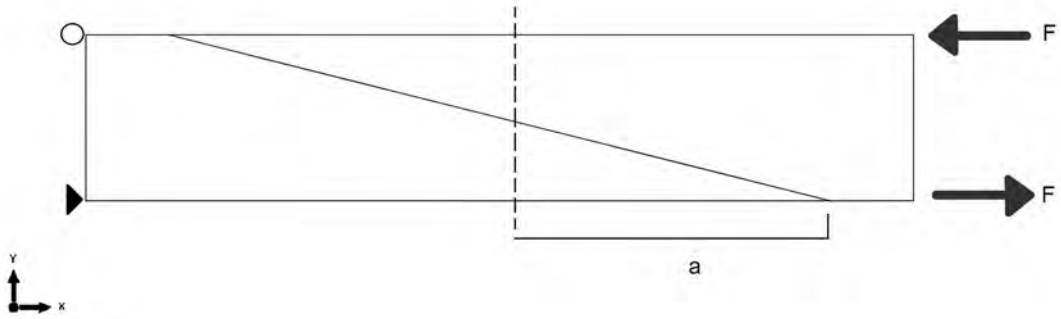

(a) Two-element beam with geometric irregularity, in pure bending. Analytic solution: $u_2 = 0.0005mm$

Results

	USER/VUEL (β=0)	USER/VUEL (β=1)	C3D8	C3D8H	C3D8R
a	U2	U2	U2	U2	U2
0	0.00049900	0.00012070	0.0001379	0.00013790	0.03538000
1	0.00023630	0.00008400	0.00008036	0.00008036	0.00523700
2	0.00012850	0.00007227	0.00005023	0.00005023	0.00148900
3	0.00007816	0.00006328	0.00003945	0.00003945	0.00070160
4	0.00008447	0.00023850	0.00003225	0.00003225	0.00045470
4.999	0.00007045	0.00013320	0.00002632	0.00002632	0.00036635

(b) Patch test 3 analysis results

Relative Error %

	USER/VUEL (β=0)	USER/VUEL (β=1)	C3D8	C3D8H	C3D8R
a	U2	U2	U2	U2	U2
0	0.2000	75.860	72.420	72.420	6976
1	52.740	83.200	83.928	83.928	947.4
2	74.300	85.546	89.954	89.954	197.8
3	84.368	87.344	92.110	92.110	40.32
4	83.106	52.300	93.550	93.550	9.060
4.999	85.910	73.360	94.736	94.736	26.73

(c) Patch test 3 relative error (percentage deviation from analytic solution)

Figure 3.7: Patch 3: Geometry description (a) and analysis results (b) , (c)

By reviewing this patch test's results it becomes obvious that the USER element with β parameter set to zero performs better than every other tested element. For the case of the uniform two-element mesh the USER element presents astonishingly small relative error while , in addition, and as depicted in 3.8 and 3.9 the USER element still exhibits reduced relative error compared to the ABAQUS explicit elements, even

for large values of the applied skew distance "a" . For specific instances where ($a > 3$) it can be observed that the reduced integrated ABAQUS element C3D8R or the USER element with β=1, achieve diminished error, however it is important to acknowledge the possibility of having better approximation of the analytic solution due to severe accuracy failure, as both of the above mentioned elements are unable to simulate the analytic solution even for the case of uniform two element mesh.

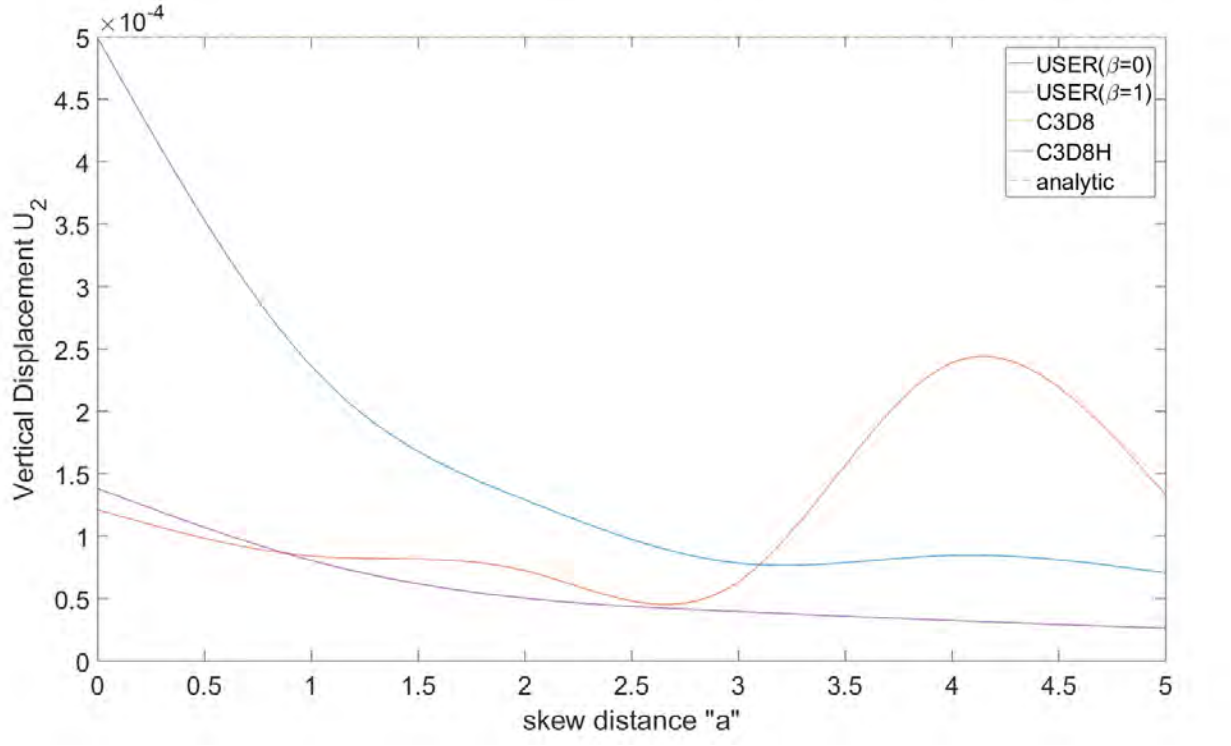

Figure 3.8: Distortion sensitivity for the USER element, as well as the ABAQUS elements C3D8, C3D8H.

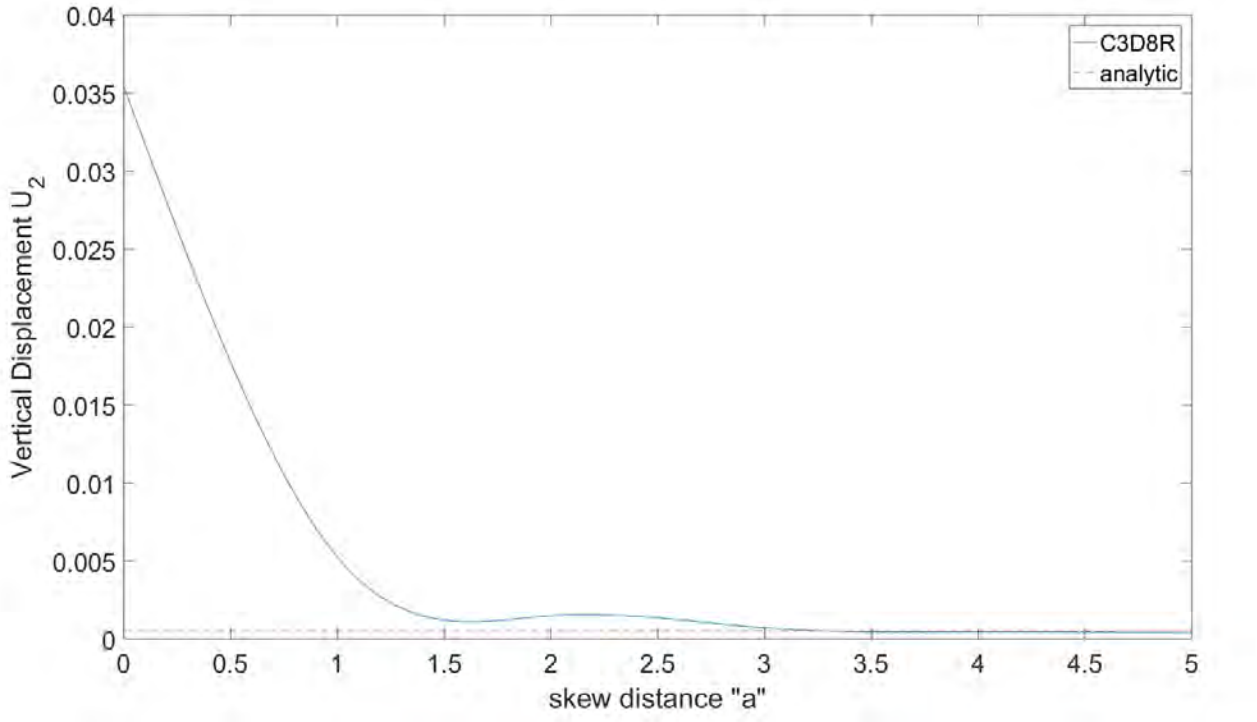

Figure 3.9: Distortion sensitivity for C3D8R (presented separately due to scaling issues caused by extreme relative error values).

3.4 Patch test 4: Cantilever beam subjected to shear tip loading

For this patch test proposed by Puso M. A., a cantilever beam is subjected to pure bending load. The material properties used are: E=$2 * 10^5$ MPa, ν=0.3, the analysis is restricted to the purely elastic region, also a vertical load F of magnitude $15 * 10^-3N$ is applied to the beam's free end and our geometry is of length=20 mm, height=2 mm as well as thickness=1 mm. As stated before, geometrical deviation from the finite element's standard shape (in the hexahedral finite element case, the standard shape is a cube) can certainly lead to accuracy failure, thus testing of irregularly shaped meshes is prioritized in the context of this specific patch test. Figure 3.10 displays all three cantilever beams tested.

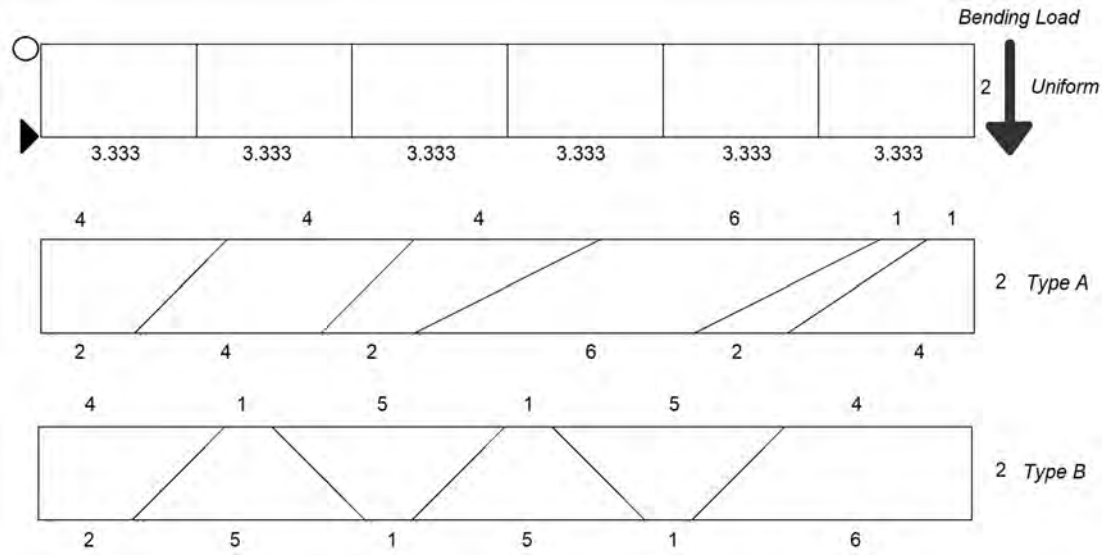

Figure 3.10: Mesh types of patch test number 4. Analytic solution: $u_2 = 0.0003mm$

	Deflection				
	USER/VUEL (β=0)	USER/VUEL (β=1)	C3D8	C3D8H	C3D8R
Uniform	0.00029970	0.00014520	0.00020410	0.00020410	0.0273900
Type A	0.00013290	0.00008456	0.00008203	0.00008202	0.0050990
Type B	0.00009747	0.00006950	0.00007930	0.00007930	0.0037090

Figure 3.11: Patch test 4 analysis results, for different element types. It is apparent that the displacement value for most of the cases is "underestimated" which essentially proves the strong presence of the shear locking phenomenon (Refer to section2.2).

	Relative Error %				
	USER/VUEL (β=0)	USER/VUEL (β=1)	C3D8	C3D8H	C3D8R
Uniform	0.100	51.600	31.967	31.967	9030
Type A	55.70	71.813	72.658	72.660	1600
Type B	67.51	76.833	73.567	73.567	1136

Figure 3.12: Solution error, percentage deviation from analytic solution

It becomes evident that for this patch test's rectangular geometry, the USER element with parameter β set to zero has to outperform the USER element with parameter β set to one. Undoubtedly the analysis results not only prove that the above statement is indeed true, but at the same time they actually underline, that when β=0 the USER element presents observably smaller relative error (percentage deviation from theoretical solution value) than every explicit ABAQUS finite element tested at any given mesh type, while at the same time the USER element demonstrates almost zero relative error for the case of the uniform mesh. Unfortunately for the instances of Type A mesh as well as Type B mesh the USER element cannot successfully encounter the severe presence of shear locking phenomenon, however it still accomplishes reduced relative error compared to the tested ABAQUS elements and especially compared to the C3D8R, a reduced integrated finite element which completely fails to simulate the accurate (according the benchmark solution) tip deflection, not only for the TYPE A mesh but also for TYPE B mesh and even for the case of the uniform mesh.

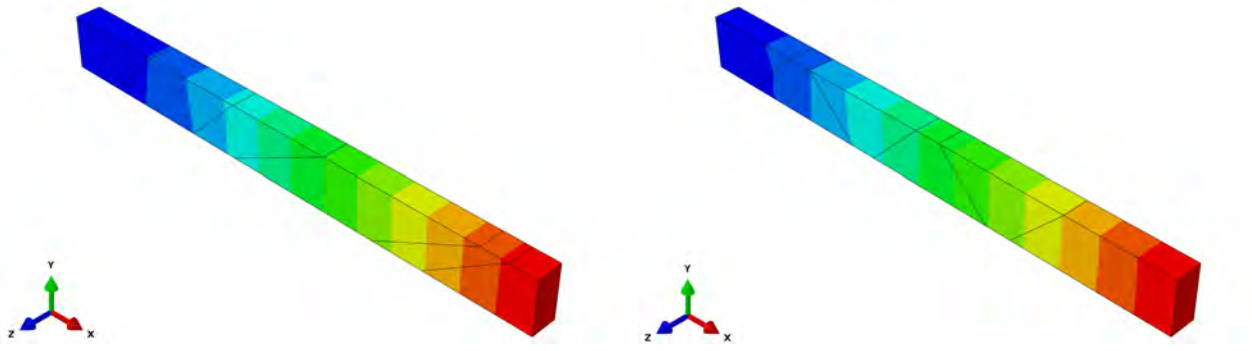

(a) Type A mesh

(b) Type B mesh

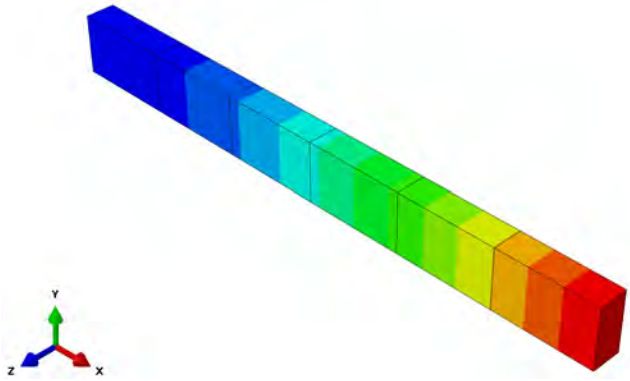

(c) Uniform mesh

Figure 3.13: Vertical deformation for different mesh types, using the USER element with $\beta = 0$

3.5 Patch test 5: Cantilever beam subjected to various loading conditions

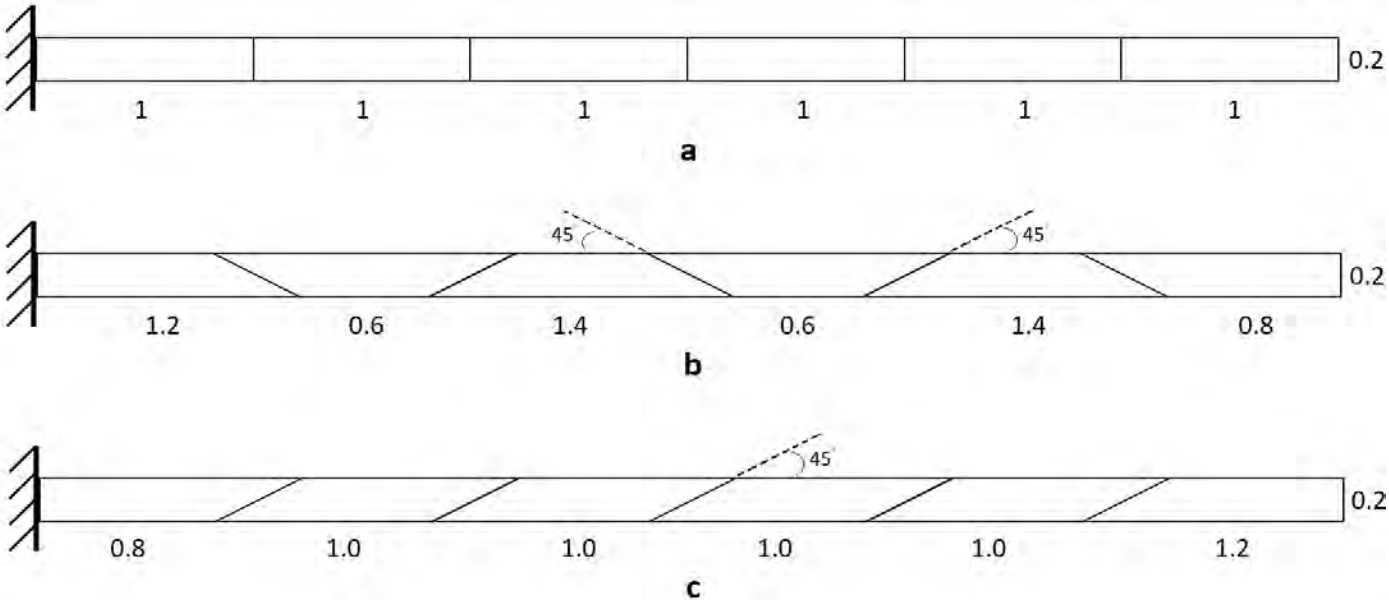

Figure 3.14: Different mesh types of this patch test's cantilever beam; (a) Uniform mesh/regular shape elements ; (b) Trapezoidal shape elements ; (c) Parallelogram shape elements

Patch test number 5, proposed by Macneal R. H. and Harder R. L., suggests that a cantilever beam of length=6.0 m; Height=0.2 m; Thickness=0.1 m is subjected to various tip loading conditions, such as extension, in-plane shear and out-of-plane shear. The material properties for our given geometry are: E=$1.0 * 10^7 Pa$; ν=0.3 and in accordance with patch test number 4 the simulation is bounded in the linear regime, while the total tip force is set at $F = 10^{-3} N$. The purpose of this particular patch test is similar to that of the previous one, as our USER element's performance is challenged through a series of different (regular or irregular) mesh types, however this analysis aims to additionally test the behavior of an elastic cantilever beam, under tensile and out-of-plane shear loading conditions, instead of solely focusing on pure bending.

In-plane Shear Deflection U2

	USER/VUEL (β=0)	USER/VUEL (β=1)	C3D8	C3D8H	C3D8R
Type A	0.00010720	0.000010520	0.000010770	0.000010770	0.00985900
Type B	0.000001953	0.000002444	0.000001960	0.000001960	0.00026690
Type C	0.000011120	0.000005877	0.000002737	0.000002737	0.00026750

Relative Error %

	USER/VUEL (β=0)	USER/VUEL (β=1)	C3D8	C3D8H	C3D8R
Type A	0.74	90.26	90.03	90.03	9028.70
Type B	98.19	97.74	98.19	98.19	147.13
Type C	89.70	94.56	97.47	97.47	147.69

Figure 3.15: Analysis results for the case of in-plane shear tip loading. Benchmark solution: $u_2 = 0.000108m$

Extension U1

	USER/VUEL (β=0)	USER/VUEL (β=1)	C3D8	C3D8H	C3D8R
Type A	0.000030020	0.000030020	0.0000300	0.0000300	0.0000300
Type B	0.000030010	0.000030010	0.0000300	0.0000300	0.0000300
Type C	0.000030010	0.000030010	0.0000300	0.0000300	0.0000300

Relative Error %

	USER/VUEL (β=0)	USER/VUEL (β=1)	C3D8	C3D8H	C3D8R
Type A	0.07	0.07	0.00	0.00	0.00
Type B	0.03	0.03	0.00	0.00	0.00
Type C	0.03	0.03	0.00	0.00	0.00

Figure 3.16: Analysis results for the case of extension. Benchmark solution: $u_1 = 0.00003m$

Out-of-Plane Shear Deflection U3

	USER/VUEL (β=0)	USER/VUEL (β=1)	C3D8	C3D8H	C3D8R
Type A	0.000424100	0.000011300	0.000011090	0.000011090	0.039420
Type B	0.000004228	0.000002728	0.000002629	0.000002629	0.001376
Type C	0.000182200	0.000003454	0.000003446	0.000003446	0.001092

Relative error %

	USER/VUEL (β=0)	USER/VUEL (β=1)	C3D8	C3D8H	C3D8R
Type A	1.83	97.38	97.43	97.43	9025.0
Type B	99.02	99.37	99.39	99.39	218.52
Type C	57.82	99.20	99.20	99.20	152.78

Figure 3.17: Analysis results forout-of-plane shear tip loading. Benchmark solution: $u_3 = 0.000432m$

As far as it concerns the cases of in-plane and out-of-plane shear tip loading the USER element exhibits great performance characteristics when it comes to the uniform mesh, however it is apparent that the relative

error rises significantly for the instances of trapezoidal or parallelogram shaped elements. Unfortunately, for the specific occasion of trapezoidal shape elements subjected to in-plane shear tip loading, it is observable that the USER element with parameter β set to one, actually, outperforms the USER element with parameter β set equal to zero, which is definitely not something that should be expected, however, both elements exhibit signs of severe shear locking phenomena which ultimately leads to accuracy failure and the above results shouldn't be taken into consideration. When the cantilever beam is subjected to tensile tip loading, it becomes clear that the ABAQUS elements present reduced relative error compared to the USER element but it can be stated that the actual performance improvement is indeed insignificant.

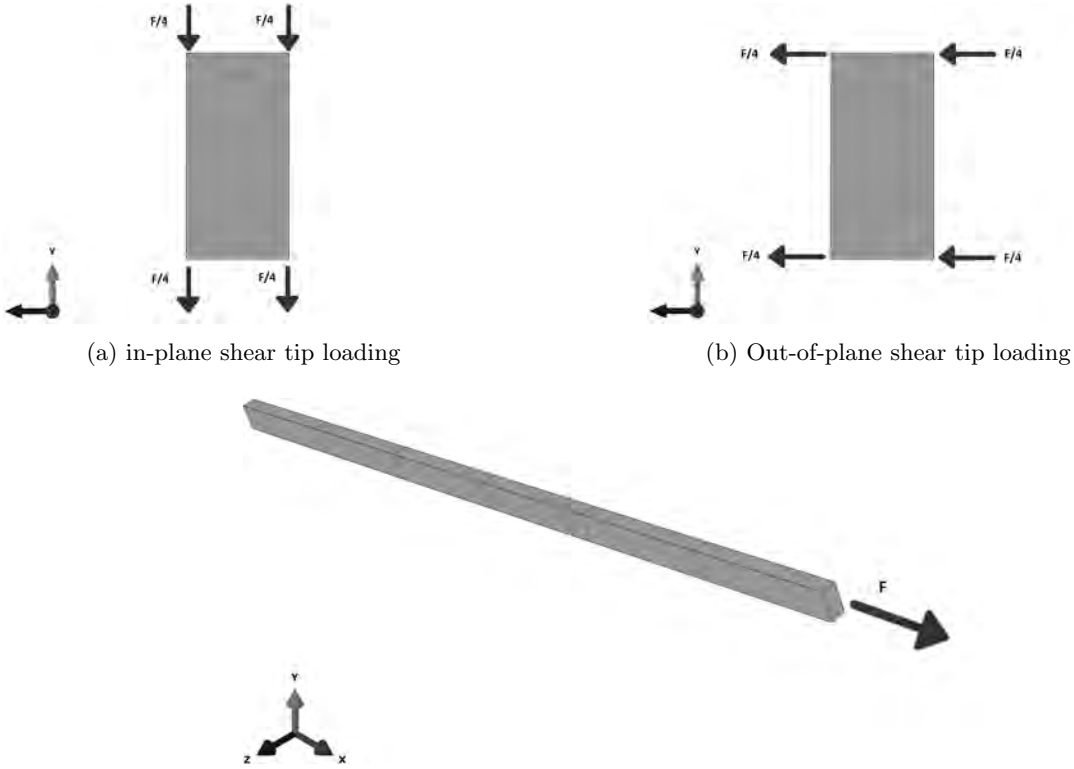

(a) in-plane shear tip loading

(b) Out-of-plane shear tip loading

(c) Tensile tip loading

Figure 3.18: Tip loading description

3.6 Patch test 6: Twisted beam under various loading conditions

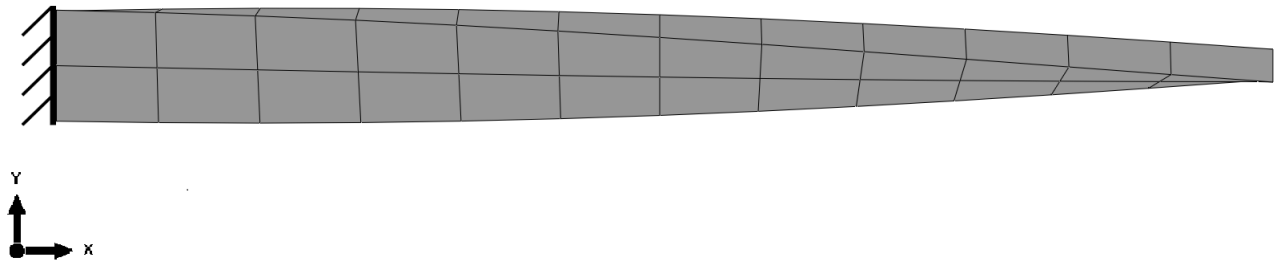

Figure 3.19: The twisted beam of patch test 6

In the context of patch test number 6, a twisted beam is subjected to pure bending as well as out-of plane shear tip loading and the displacement in the direction of the implemented force is measured and eventually correlated to the analytic solution. Our beam is of length=12.0 mm; height=1.1 mm; thickness=0.32 mm and presents a twist of 90° (root to tip). Furthermore, the elastic material properties are set at: $E = 29.0 * 10^5 MPa$; $\nu = 0.22$ and a 12x2x1 computational mesh is utilized.

Dissimilar to the straight beam problem, for the case of the curved cantilever beam, variations of the principal deformation modes can be elicited by pure shear loading conditions (in-plane-shear or out-of plane

shear at tip). Note that this particular patch test is the only one in this thesis' applications section, which essentially tests the effect of warp on hexahedral elements, as a twist of 7.5° is exhibited at each element of the beam. In addition, it is certain that the element's shape is far from a normal cube (the standard shape for our hexahedral finite element) which will essentially assist in the examination of the effect of shape irregularity in the analysis accuracy. Notice that the reference solution utilized for error estimation purposes is suggested by Macneal R. H. and Harder R. L.. Of course newer theories such as the linearized three-dimensional beam theory proposed by Zupan D. and Saje M. reach an analytic result for the material linear regime but their deviation from MacNeal's solution is definitely insignificant.

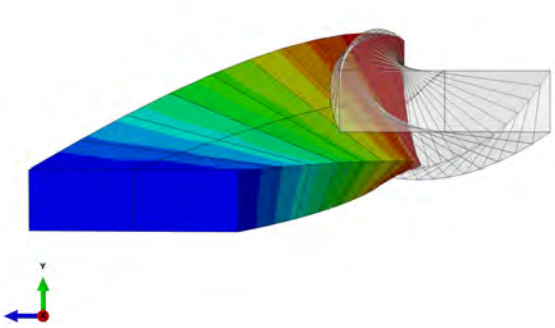

(a) Deformed result for twisted beam subjected to out-of-plane shear. Scale factor=300

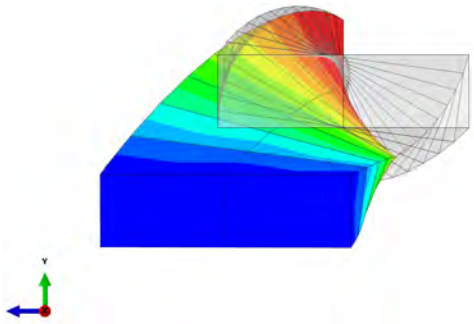

(b) Deformed result for twisted beam subjected to in-plane shear. Scale factor=300

Figure 3.20: Deformed results for patch 6

Analysis results, prove that the USER element (with $\beta = 0$) does not exhibit any signs of accuracy failure even in the event of warped and heavily irregular shaped elements .It is obvious that both for the case of out-of-plane shear and that of in-plane shear tip loading the USER element's performance is spectacular as the error (percentage deviation from benchmark solution) is almost zero, while, in contrary, the tested ABAQUS elements fail to keep up with the twisted geometry of patch six's cantilever beam.

Tip Deflection U2

Element	USER/VUEL (β=0)	USER/VUEL (β=1)	C3D8	C3D8H	C3D8R
U2	0.00173800	0.00059200	0.00064550	0.00006455	0.16010000

Relative Error %

Element	USER/VUEL (β=0)	USER/VUEL (β=1)	C3D8	C3D8H	C3D8R
U2	0.91	66.25	63.20	96.32	9027.71

Figure 3.21: Patch 6 results for the case of in-plane shear tip loading. MacNeal's Benchmark solution: $u_2 = 0.001754mm$. Zupan's Benchmark solution: $u_2 = 0.001749mm$

Tip deflection U3

Element	USER/VUEL (β=0)	USER/VUEL (β=1)	C3D8	C3D8H	C3D8R
U3	0.00541900	0.00111400	0.00126300	0.00126300	0.45330000

Relative Error %

Element	USER/VUEL (β=0)	USER/VUEL (β=1)	C3D8	C3D8H	C3D8R
U3	0.09	79.46	76.71	76.71	8257.30

Figure 3.22: Patch 6 results for the case of out-of-plane shear tip loading. MacNeal's Benchmark solution: $u_3 = 0.005424mm$. Zupan's Benchmark solution: $u_3 = 0.005429mm$

3.7 Patch test 7: Cyclic loading of a cantilever beam

As Puso M. A. mentions, incremental methods occasionally exhibit remaining-permanent deformation, when an elastic material is loaded and unloaded, which is indeed a negative numerical phenomenon with no physical meaning. Thus, it becomes important that our problem set features a patch test that evaluates the performance of our USER element in the event of cyclic loading. For the needs of patch test number 7, a straight cantilever beam of length=10m; Height=1m; depth=1m is used, the elastic material properties are set to E=20GPa($\equiv 2*10^{10}$Pa); $\nu = 0.4$ and the analysis is restricted to the purely linear deformation regime (Green-St. Venant material model).At first, a 6x2x1 coarse mesh is used, however later, a fine 45x8x8 mesh is established and the problem is run explicitly using a large number of time increments (approximately $10*6$), for convergence validation purposes. Ultimately, for this example, a beam is subjected to an axial load, then a shear load and finally unloaded, with the loading sequence being as follows:

(1)The axial load is ramped up from P=0 to P=$2*10^4N$ and eventually deformed by $u_1 = 0.101319m$ (USER element with $\beta = 0$) at time $t = 3.3*10^{-3}s$, while the vertical load V, is set at zero.
(2)The axial load P remains at P=$2*10^4N$ and the vertical load is ramped up from V=0 to V=$50N$ at time $t = 6.6*10^{-3}s$. We can calculate the total deformation at the end of step 2 as: $u_1 = 0.101248m$ and $u2 = 0.0.0364161m$ (USER element with $\beta = 0$)
(3)From $t = 6.6*10^{-3}s$ to $t = 10^{-2}s$ both the shear and axial forces are removed (ramped down). Spurious/permanent deflection at this point is not observable as depicted at Figure 3.23 (c). However a minimal amount of remaining total deformation can still be calculated as : $u_1 = -1.96592*10^{-7}m$ and $u2 = 0.0.000131642m$.
Notice that P and V retain their orientation with respect to the global coordinate system for the whole duration of the simulation.

Prior to proceeding to the test results, acknowledge that this particular analysis is time independent, thus the time duration of each step won't affect our simulation results. Of course, in the event that the user desires to obtain a solution for rate-dependent material models (viscoelastic materials for example) , it becomes clear that step duration should be thoroughly considered.

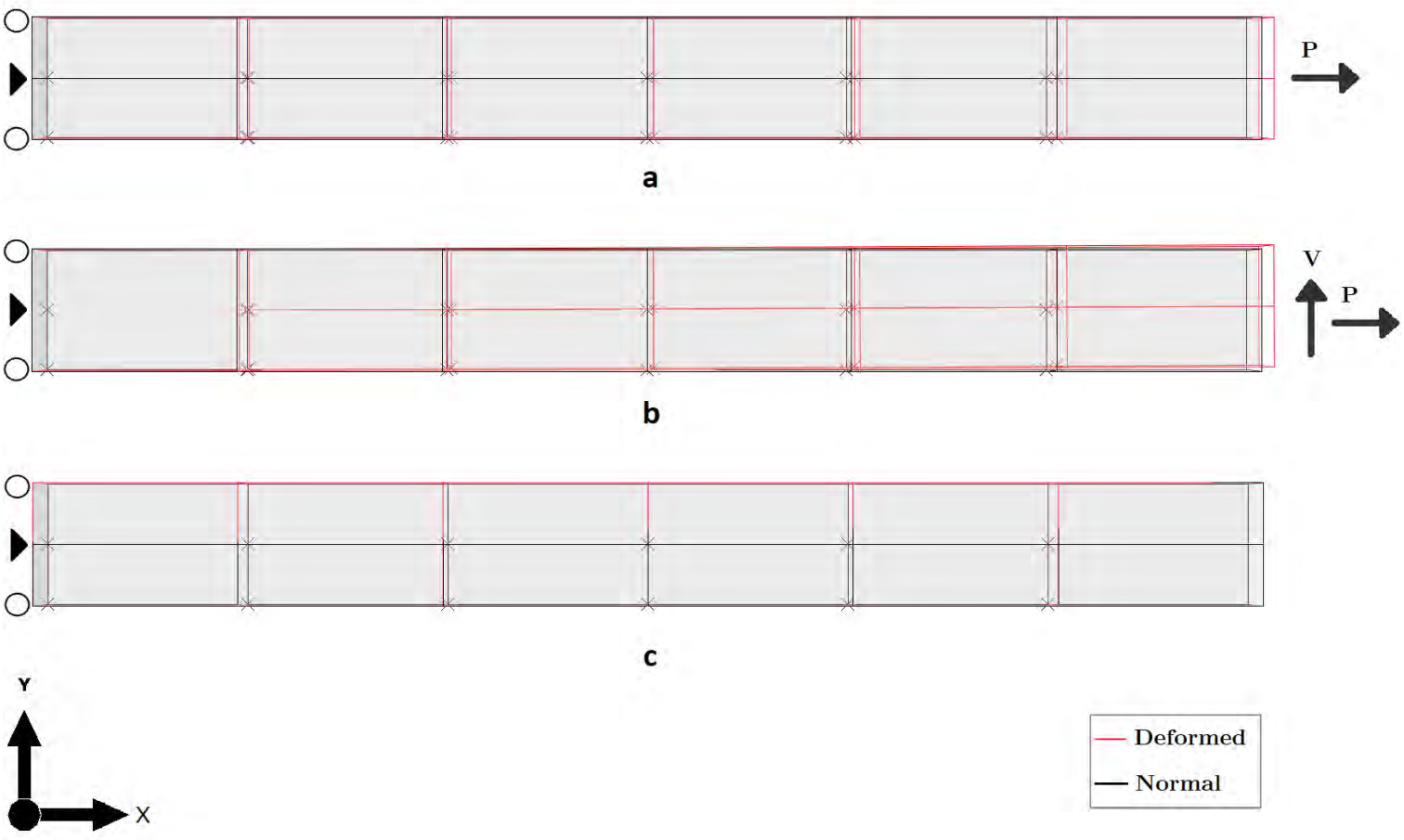

Figure 3.23: (a) Description of the beam for $t = 3.3*10^{-3}s$. ; (b) Beam for $t = 6.6*10^{-3}s$.; (c) Final shape of the beam. Spurious deformation is not visible.; Deformation Scale factor=1 for every instance.

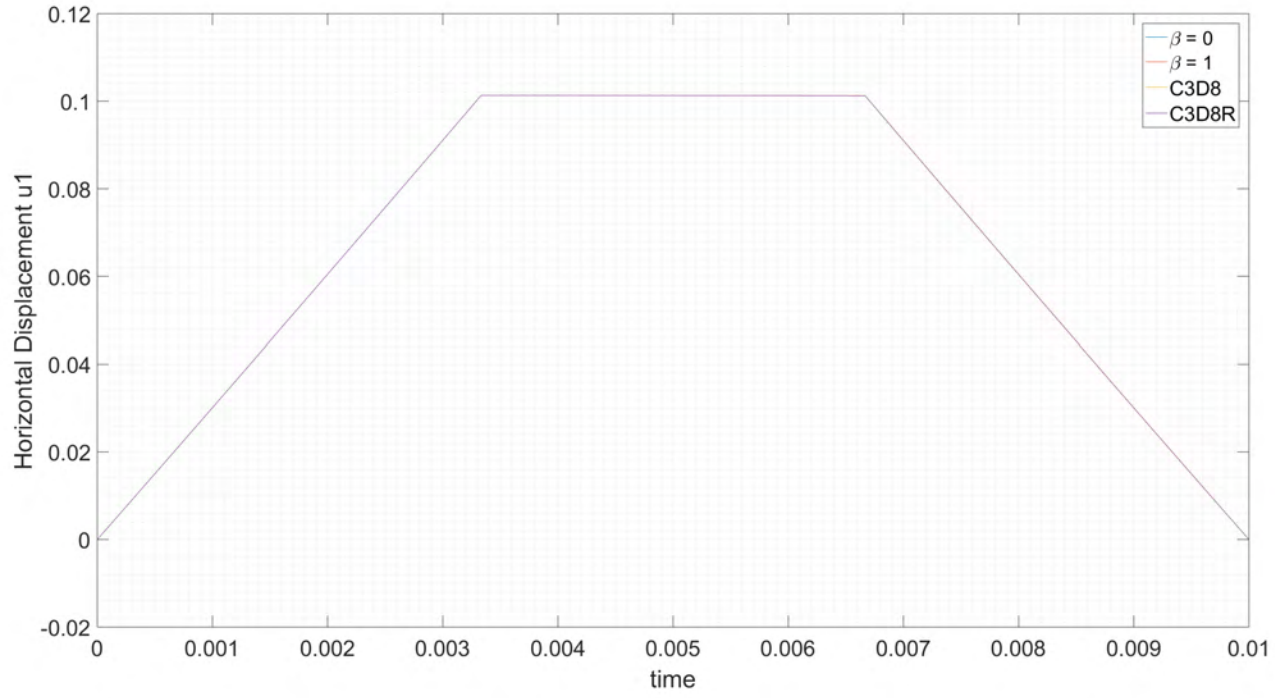

Figure 3.24: Horizontal Deflection u_1 vs analysis time

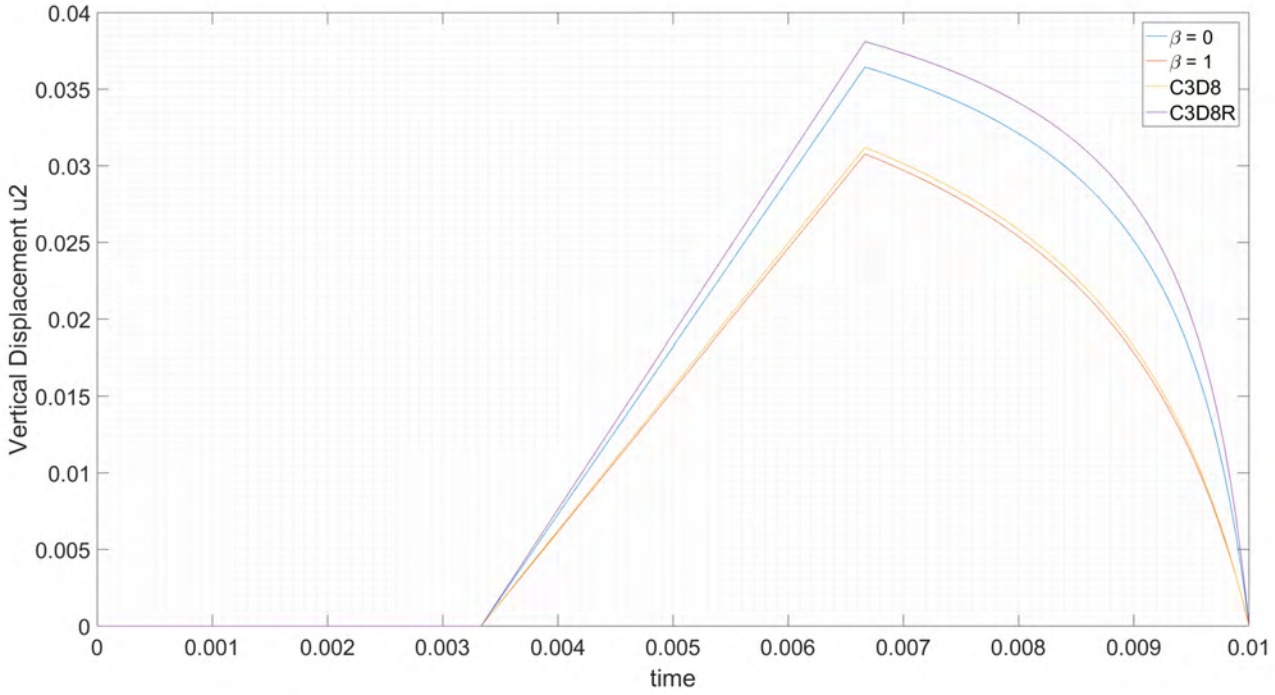

Figure 3.25: Vertical Deflection u_2 vs analysis time

Every tested element exhibits a certain amount of permanent vertical as well as horizontal deformation, however the ammount of remaining distortion succeeding the unloading is truly insignificant when correlated to the maximum value of shear or tensile deformation respectively. It is clear that the Abaqus elements perform really well, but especially for the case of our USER element (with $\beta = 0$), the magnitude of permanent shear deformation (which according to Puso M. A. is the most critical factor that has to be thoroughly examined in the context of this patch test) is sensibly reduced compared to that of C3D8. Also, signs of shear locking are indeed observable for the instances of the USER element (with $\beta = 1$) as well as the C3D8R ABAQUS element and of course, it can be stated that the value of permanent spurious deformation

is actually analogous to the intensity of the shear locking phenomenon.Note that the analysis is run explicitly for ABAQUS elements C3D8 , however the C3D8H is not support by the explicit solver, thus an implicit simulation is performed for this specific element.

Absolute percentage difference for U1

USER(β=0)	USER(β=1)	C3D8	C3D8R
-0.000001940	0.000000236	-0.000000013	0.000003172

Figure 3.26: Absolute percentage difference for horizontal deflection u_1 (Maximum value/End Value)

Absolute percentage difference for U2

USER(β=0)	USER(β=1)	C3D8	C3D8R
0.003611409	0.003676323	0.000044062	0.001896279

Figure 3.27: Absolute percentage difference for vertical deflection u_2 (Maximum value/End Value)

3.8 Patch test 8: Necking of a tensile specimen

It has been sporadically reported that a variety of elements using the enhanced assumed strain hourglass control techniques, exhibit problematic behavior when loaded in the large tensile strain regime. In order to examine if the above statement applies to our USER element, a plain strain bar of length=100 mm ; diameter=24 mm is utilized and it can be observed that the computational mesh is finer at the tip than the base of the bar. Of course this linear perturbation is implemented in our geometry, in the direction of initiating and eventually accelerating the process of necking of our tensile specimen. Eventually, the strain bar is constrained at its bottom end, while a displacement of magnitude $u_2 = 30mm$ is applied on its tip. Notice that a power law plasticity model of type:

$$\sigma_y\left(\bar{\varepsilon}^p\right) = \sigma_0\left(1+\frac{\bar{\varepsilon}^p}{\varepsilon_0}\right)^{1/n}, \qquad \varepsilon_0 = \frac{\sigma_0}{E} \tag{3.1}$$

is used and the material constants for this patch test are: Young's Modulus E=$2*10^5 MPa$; Poisson's constant $\nu = 0.3$; Yield strength σ_0=200MPa; Density $\rho = 7.85 \cdot 10^{-9} \frac{N\,s^2}{mm^4}$ as well as hardening exponent n=10. Note that the analysis is rate independent and additionally that effects of temperature are neglected.

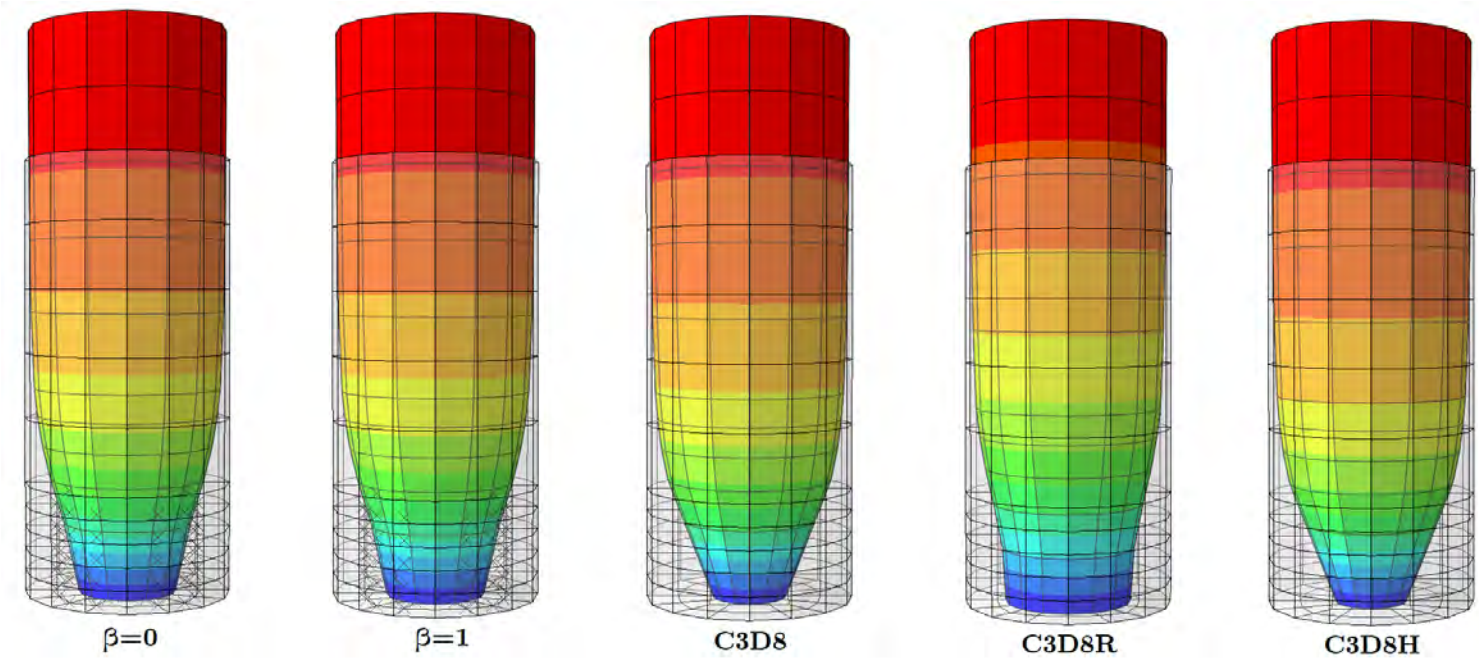

Figure 3.28: Deformation visualization for different parameter β options of the USER element.

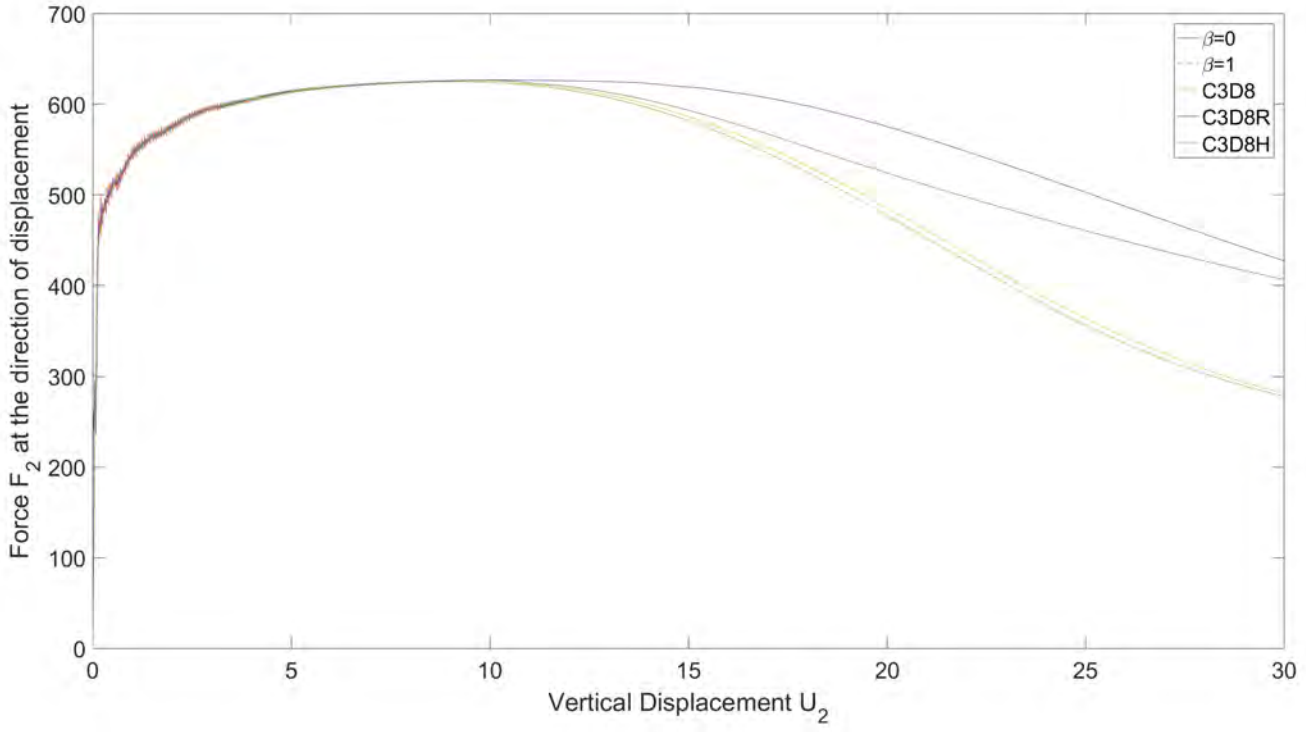

Figure 3.29: Force-displacement diagram for tested elements. Noise/oscillations for the user elements are due to the usage of ABAQUS explicit solver.

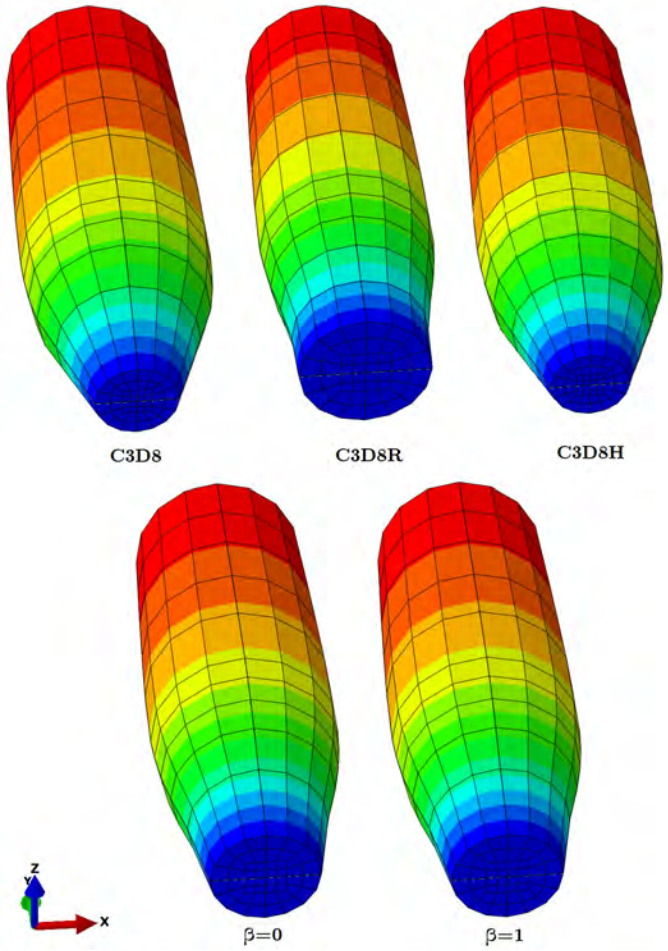

Figure 3.30: Strain bar deformation for different elements.

Figure 3.29 shows that the USER element as well as the ABAQUS element C3D8 actually perform well in the large strain tensile regime, however the C3D8R exhibits signs of volumetric locking. Furthermore, our analysis results prove that the ABAQUS element C3D8H, which introduces a supplementary degree of freedom - the hydrostatic pressure p, operates excellent and with reduced signs of volumetric locking that the other tested elements. Ultimately it can be acknowledged that the non-linear simulations lead to identical results for the cases of $\beta = 0$ as well as $\beta = 1$ and this behavior is definitely expected as the β is introduced to address the undesirable phenomenon of shear locking. Of course in the context of this patch problem, our strain bar is subjected to pure tensile load, thus the absence of shear deformation secures that shear locking is not probable to emerge.

Conclusions

It becomes obvious that the introduction of non-local plasticity e^p, to the set of primary nodal unknowns in finite element analysis,certainly resolves the disastrous phenomenon of solution dependence on the direction as well as fineness of the computational mesh. At the same time, the enhanced-assumed strain method for hourglass control provides a non-arbitrary (in contrast to the "classic" hourglass control models) solution to the rise of spurious modes. Unfortunately, even when a proper theoretical basis is established in finite element formulation, the user elements suffer from certain types of accuracy failure, with the shear as well as volumetric phenomena certainly being the most characteristic ones.

Thus, in the direction of validating the quality of simulation associated with our hexahedral brick, a series of demanding patch tests is performed on the user element as well as the commercial elements C3D8,C3D8H and C3D8R, and ultimately the analysis results are correlated with the corresponding benchmark solutions. By taking into consideration the patch tests executed in the context of this thesis, it can be stated that for most of the cases, and with a comprehensive selection for the value of β parameter, the newly-proposed finite element performs indeed well and noticeably better than the commercial, ABAQUS elements. Obviously the USER element operates well in the linear, as well as the plastic material regime, however it exhibits signs of accuracy failure when tested in elastic problems with heavily distorted meshes but, undoubtedly, this phenomenon certainly affects most of user or commercial finite element formulations. Fortunately the numerical analysis' results remain trustworthy for moderately wrapped elements and additionally, the user element presents minor to neglectable volumetric locking when tested in the large plastic strain region, where necking occurs.

Appendix

A.1 Average Matrices and stabilization forces

as proposed by Flanagan D. P. and Belytschko T.:

$$\underset{9\times 24}{\overline{[\mathbf{B}_L(\xi)]}} = \left[\begin{array}{cccc} \underset{9\times 3}{\overline{\left[\mathbf{B}_L^{(1)}\right]}} & \underset{9\times 3}{\overline{\left[\mathbf{B}_L^{(2)}\right]}} & \cdots & \underset{9\times 3}{\overline{\left[\mathbf{B}_L^{(8)}\right]}} \end{array} \right] \tag{A.1}$$

$$\underset{9\times 3}{\overline{\left[\mathbf{B}_L^{(A)}\right]}} = \begin{bmatrix} (\bar{\mathbf{b}}_1)_A & 0 & 0 \\ 0 & (\bar{\mathbf{b}}_2)_A & 0 \\ 0 & 0 & (\bar{\mathbf{b}}_3)_A \\ (\bar{\mathbf{b}}_2)_A & 0 & 0 \\ 0 & (\bar{\mathbf{b}}_1)_A & 0 \\ (\bar{\mathbf{b}}_3)_A & 0 & 0 \\ 0 & 0 & (\bar{\mathbf{b}}_1)_A \\ 0 & (\bar{\mathbf{b}}_3)_A & 0 \\ 0 & 0 & (\bar{\mathbf{b}}_2)_A \end{bmatrix} \qquad A = 1,2,3,4,5,6,7,8 \tag{A.2}$$

$$\underset{8\times 1}{\overline{\{\mathbf{b}_i\}}} = \frac{1}{V_e}\int_{\Omega^e} \frac{\partial}{\partial x_i}\underset{8\times 1}{\{\mathbf{N}\}}\, d\Omega \qquad i = 1,2,3 \tag{A.3}$$

A.2 Strains in natural space

For the natural space (x,n,ζ) we define: (as mentioned by Simo J. C. and Rifai M. S.)

$$\Delta\tilde{L}_{ij} = \frac{J}{J_0}(\mathbf{J}_0)_{mi}(\mathbf{J}_0)_{nj}\Delta L_{mn}, \quad \Delta\tilde{u}_i^A = (\mathbf{J}_0)_{ki}\,\Delta u_k^A \tag{A.4}$$

$$(J_0)_{ik} = \left.\frac{\partial x_i}{\partial \xi_k}\right|_{\boldsymbol{\xi}=\mathbf{0}}, \quad j_{ik} = \left(\mathbf{J}_0^{-1}\right)_{ik} = \left.\frac{\partial \xi_i}{\partial x_k}\right|_{\boldsymbol{\xi}=\mathbf{0}} \tag{A.5}$$

and note that

$$\Delta L_{ij} = \frac{J_0}{J} j_{mi}\, j_{nj}\, \Delta\tilde{L}_{mn}, \quad \Delta u_i^A = j_{ki}\,\Delta\tilde{u}_k^A \tag{A.6}$$

In matrix form

$$\left(\underset{9\times 9}{[\mathbf{K}_0]} = \underset{9\times 9}{\left[\mathbf{J}_0^{-1}\right]} \right)$$

$$\underset{9\times 1}{\left\{\Delta\tilde{\mathbf{L}}\right\}} = \frac{J}{J_0}\underset{9\times 9}{[\mathbf{J}_0]}\underset{9\times 1}{\{\Delta\mathbf{L}\}}, \qquad \underset{9\times 1}{\{\Delta\mathbf{L}\}} = \frac{J_0}{J}\underset{9\times 9}{[\mathbf{K}_0]}\underset{9\times 1}{\left\{\Delta\tilde{\mathbf{L}}\right\}} \tag{A.7}$$

and

$$\underset{3\times1}{\left\{\Delta\tilde{\mathbf{u}}_{e,i}^{N}\right\}}=\underset{3\times3}{\left[\mathbf{J}_0\right]^T}\underset{24\times1}{\left\{\Delta\mathbf{u}_{e,i}^{N}\right\}},\qquad\underset{24\times1}{\left\{\Delta\tilde{\mathbf{u}}_{e}^{N}\right\}}=\underset{24\times24}{[G]}\underset{24\times1}{\left\{\Delta\mathbf{u}_{e}^{N}\right\}}\tag{A.8}$$

where

$$\underset{24\times24}{[G]}=\begin{bmatrix}\underset{3\times3}{\left[\mathbf{J}_0\right]^T} & & \\ & \ddots & \\ & & \underset{3\times3}{\left[\mathbf{J}_0\right]^T}\end{bmatrix}\tag{A.9}$$

Finally we can write:

$$\underset{9\times1}{\left\{\Delta\tilde{\mathbf{L}}\right\}}=\underset{9\times24}{\left[\tilde{\mathbf{B}}\right]}\underset{24\times1}{\left\{\Delta\tilde{\mathbf{u}}_{e}^{N}\right\}},\quad\underset{9\times24}{\left[\tilde{\mathbf{B}}\right]}=\frac{J}{J_0}\underset{9\times9}{\left[\mathbf{J}_0\right]}\underset{9\times24}{\left[\mathbf{B}\right]}\underset{24\times24}{\left[G\right]^{-1}},\quad or\quad\underset{9\times24}{\left[\mathbf{B}\right]}=\frac{J_0}{J}\underset{9\times9}{\left[\mathbf{K}_0\right]}\underset{9\times24}{\left[\tilde{\mathbf{B}}\right]}\underset{24\times24}{[G]}\tag{A.10}$$

A.3 Stabilization matrices at natural space

Definition for shape functions:

$$\underset{8\times1}{\left\{\mathbf{N}\left(\xi\right)\right\}}=\frac{1}{8}\left(\underset{8\times1}{\left\{\mathbf{s}\right\}}+\sum_{j=1}^{3}\xi_j\underset{8\times1}{\left\{\xi_j\right\}}+\sum_{k=1}^{4}h_k\left(\xi\right)\underset{8\times1}{\left\{\mathbf{h}_k\right\}}\right)\tag{A.11}$$

where $\underset{8\times1}{\{\xi_i\}},\quad(i=1,2,3)$, or alternatively

$$\underset{8\times1}{\left\{\mathbf{N}\left(\mathbf{x}\right)\right\}}=\underset{8\times1}{\left\{\mathbf{b}_0\right\}}+\sum_{j=1}^{3}\underset{8\times1}{\left\{\mathbf{b}_j\right\}}x_j+\sum_{k=1}^{4}h_k\left(\xi\left(\mathbf{x}\right)\right)\underset{8\times1}{\left\{\gamma_k\right\}}\tag{A.12}$$

$$\underset{1\times8}{\left\lfloor\mathbf{s}\right\rfloor}=\begin{bmatrix}1&1&1&1&1&1&1&1\end{bmatrix}\tag{A.13}$$

$$h_1\left(\xi\right)=\xi_1\,\xi_2,\quad h_2\left(\xi\right)=\xi_2\,\xi_3,\quad h_3\left(\xi\right)=\xi_3\,\xi,\quad h_4\left(\xi\right)=\xi_1\,\xi_2\,\xi_3\tag{A.14}$$

$$\underset{1\times8}{\left\lfloor\mathbf{h}_1\right\rfloor}=\begin{bmatrix}1&-1&1&-1&1&-1&1&-1\end{bmatrix},\quad\underset{1\times8}{\left\lfloor\mathbf{h}_2\right\rfloor}=\begin{bmatrix}1&1&-1&-1&-1&-1&1&1\end{bmatrix}\tag{A.15}$$

$$\underset{1\times8}{\left\lfloor\mathbf{h}_3\right\rfloor}=\begin{bmatrix}1&-1&-1&1&-1&1&1&-1\end{bmatrix},\quad\underset{1\times8}{\left\lfloor\mathbf{h}_4\right\rfloor}=\begin{bmatrix}-1&1&-1&1&1&-1&1&-1\end{bmatrix}\tag{A.16}$$

We utilize the second term of A.12 to define the stabilization matrices $\underset{9\times3}{\left[\tilde{\mathbf{B}}_A\left(\xi\right)\right]}$ so as:

$$\underset{8\times1}{\tilde{\mathbf{N}}\left(\xi\right)}\equiv\sum_{i=1}^{4}h_i\left(\xi\right)\underset{8\times1}{\gamma_i}\quad or\quad\tilde{N}^A\left(\xi\right)\equiv\sum_{i=1}^{4}h_i\left(\xi\right)\gamma_i^A\quad A=1,2,3,4,5,6,7,8\tag{A.17}$$

$$\underset{9\times3}{\left[\tilde{\mathbf{B}}_{\text{stab}}^{A}\left(\xi\right)\right]}=\begin{bmatrix}\eta\,\gamma_1^A+\zeta\,\gamma_3^A+\eta\,\zeta\,\gamma_4^A & 0 & 0\\ 0 & \xi\,\gamma_1^A+\zeta\,\gamma_2^A+\zeta\,\xi\,\gamma_4^A & 0\\ 0 & 0 & \eta\,\gamma_2^A+\xi\,\gamma_3^A+\xi\,\eta\,\gamma_4^A\\ \underline{\xi\,\gamma_1^A}+\zeta\,\gamma_2^A+\underline{\zeta\,\xi\,\gamma_4^A} & 0 & 0\\ 0 & \underline{\eta\,\gamma_1^A}+\zeta\,\gamma_3^A+\underline{\eta\,\zeta\,\gamma_4^A} & 0\\ \eta\,\gamma_2^A+\underline{\xi\,\gamma_3^A}+\underline{\xi\,\eta\,\gamma_4^A} & 0 & 0\\ 0 & 0 & \eta\,\gamma_1^A+\underline{\zeta\,\gamma_3^A}+\underline{\eta\,\zeta\,\gamma_4^A}\\ 0 & \underline{\eta\,\gamma_2^A}+\xi\,\gamma_3^A+\underline{\xi\,\eta\,\gamma_4^A} & 0\\ 0 & 0 & \xi\,\gamma_1^A+\underline{\zeta\,\gamma_2^A}+\underline{\zeta\,\xi\,\gamma_4^A}\end{bmatrix}\tag{A.18}$$

and finally we get:

$$\underset{9\times 24}{\left[\tilde{\mathbf{B}}_{\text{stab}}(\xi)\right]} = \sum_{i=1}^{4} \underset{9\times 3}{\left[\hat{\mathbf{B}}_i(\xi)\right]} \underset{3\times 24}{[\mathbf{\Gamma}_i]^T} \qquad \underset{24\times 3}{[\mathbf{\Gamma}_i]} = \begin{bmatrix} \gamma_i^1 \underset{3\times 3}{[\delta]} \\ \gamma_i^2 \underset{3\times 3}{[\delta]} \\ \vdots \\ \gamma_i^8 \underset{3\times 3}{[\delta]} \end{bmatrix} \tag{A.19}$$

A.4 Useful formulas/equations

$$\underbrace{\underset{3\times 24}{[\mathbf{\Gamma}_i]^T} \underset{24\times 24}{[G]}}_{3\times 24} = \underbrace{\underset{3\times 3}{[\mathbf{J}_0]^T} \underset{3\times 24}{[\mathbf{\Gamma}_i]^T}}_{3\times 24}, \qquad \underbrace{\underset{24\times 24}{[G]^T} \underset{24\times 3}{[\mathbf{\Gamma}_i]}}_{24\times 3} = \underbrace{\underset{24\times 3}{[\mathbf{\Gamma}_i]} \underset{3\times 3}{[\mathbf{J}_0]}}_{24\times 3} \tag{A.20}$$

$$\underset{3\times 3}{[\mathbf{J}_0]} = \underset{3\times 3}{[\mathbf{J}]_{\xi=\mathbf{0}}} = \begin{bmatrix} J_{11} & J_{12} & J_{13} \\ J_{21} & J_{22} & J_{23} \\ J_{31} & J_{32} & J_{33} \end{bmatrix}_{\xi=\mathbf{0}} = \begin{bmatrix} \underset{3\times 1}{\{\mathbf{j}_1\}} & \underset{3\times 1}{\{\mathbf{j}_2\}} & \underset{3\times 1}{\{\mathbf{j}_3\}} \end{bmatrix} \tag{A.21}$$

$$\underset{3\times 3}{[\mathbf{j}_0]} = \underset{3\times 3}{[\mathbf{j}]_{\xi=\mathbf{0}}} = \underset{3\times 3}{\left([\mathbf{J}]^{-1}\right)_{\xi=\mathbf{0}}} \cong \begin{bmatrix} j_1 & & \\ & j_2 & \\ & & j_3 \end{bmatrix} = \begin{bmatrix} \frac{1}{|\mathbf{j}_1|} & & \\ & \frac{1}{|\mathbf{j}_2|} & \\ & & \frac{1}{|\mathbf{j}_3|} \end{bmatrix} \tag{A.22}$$

$$[j_1 = \frac{1}{\sqrt{\sum_{k=1}^{3} J_{k1}^2|_{\xi=\mathbf{0}}}}, \quad j_2 = \frac{1}{\sqrt{\sum_{k=1}^{3} J_{k2}^2|_{\xi=\mathbf{0}}}}, \quad j_3 = \frac{1}{\sqrt{\sum_{k=1}^{3} J_{k3}^2|_{\xi=\mathbf{0}}}} \tag{A.23}$$

ultimately, we end up with:

$$\underset{9\times 9}{[\mathbf{K}_0]} = \text{diagonal}\left\{ \begin{array}{ccccccccc} j_1^2 & j_2^2 & j_3^2 & j_1\,j_2 & j_1\,j_2 & j_1\,j_3 & j_1\,j_3 & j_2\,j_3 & j_2\,j_3 \end{array} \right\} \tag{A.24}$$

Bibliography

Aifantis E. C. 'The physics of plastic deformation'. *Int. J. Plast.*, 3(1987):211–247, a.

Aifantis E. C. 'On the role of gradients in the localization of deformation and fracture'. *Int. J. Engrg. Sci.*, 30(1992):1279–1300, b.

Aifantis E. C. 'Strain gradient interpretation of size effects'. *Int. J. Fracture*, 95(1999):299–314, c.

Anand L., Aslan O. , Chester S. A. 'A Large-deformation gradient theory for elastic-plastic materials: Strain softening and regularization of shear bands'. *Int. J. Plast.*, 30-31(2012):116–143.

Areias P. M. A. , César de Sá J. M. A., Conceiação C. A. and Fernandes A. A. 'Analysis of 3D problems using a new enhanced strain hexahedral element'. *Int. J. Num. Meth. Engrg.*, 58(2003):1637–1682.

Auricchio F. and Taylor R. L. 'A return-map algorithm for general associative isotropic elasto-plastic materials in large deformation regimes'. *Int. J. Plast.*, 15(1999):1359–1378.

Belytschko T. , Ong J. S. , Liu W.K. and Kennedy J. M. 'Hourglass control in linear and nonlinear problems'. *Comp. Methods Appl. Mech. Engrg.*, 53(1985):13–46.

Belytschko T. and Bindeman L. P. 'On the numerical integration of three-invariant elastoplastic constitutive models'. *Comp. Methods Appl. Mech. Engrg.*, 88(1988):311–340.

Belytschko T. and Binderman L. P. 'Assumed strain stabilization of the eight node hexahedral'. *Comp. Methods Appl. Mech. Engrg.*, 105(1993):225–260.

Češarek P. , Saje M. and Zupan D. 'Kinematically exact curved and twisted strain-based beam'. *Int. J. Sol. Struct.*, 49(2012):1802–1817.

de Borst R. , Mühlaus H. B. and Pamin J. 'Fundamental issues in finite element analyses of localization of deformation'. *Engrg. Comp.*, 10(1990):99–121.

de Borst R. and Mühlaus H. B. 'Gradient-dependent plasticity: Formulation and algorithmic aspects'. *Int. J. Num. Meth. Engrg.*, 35(1992):521–539.

de Borst R. and Pamin J. 'Some novel developments in finite element procedures for gradient-dependent plasticity'. *Int. J. Num. Meth. Engrg.*, 39(1996):2477–2505.

Engelen R. A. B. , Geers M. G. D. , and Baaijens F.P.T. 'Nonlocal implicit gradient-enhanced elasto-plasticity for the modelling of softening behaviour'. *Int. J. PLast.*, 19(2003):403–433.

Flanagan D. P. and Belytschko T. 'A uniform strain hexahedron and quadrilateral with orthogonal hourglass control'. *Int. J. Num. Meth. Engrg.*, 17(1981):679–706.

Freischläger C. and Schweizerhof K. 'On the systematic development of trilinear three-dimensional solid elements based on Simo's enhanced strain formulation'. *Int. J. Sol. Struct.*, 33(1996):2993–3017.

Gruben G.,Morin D. , Langseth M. and Hopperstad O. S. 'Strain localization and ductile fracture in advanced high-strength steel sheets'. *Europ. J. Mech. Sol.*, 61(2017):315–329.

Hughes T. J. R. and Winget J. 'Finite rotation effects in numerical integration of rate constitutive equations arising in large-deformation analysis'. *Int. J. Num. Meth. Engrg.*, 15(1980):1862–1867.

Koh B. C. and Kikuchi N. 'New improved hourglass control for bilinear and trilinear elements in anisostropic linear elasticity'. *Comp. Methods Appl. Mech. Engrg.*, 65(1987):1–46.

Liu W. K. , Ong J. S. and Uras R. A. 'Fininte Element stabilization matrices–a unification approach'. *Comp. Methods Appl. Mech. Engrg.*, 53(1985):13–46.

Macneal R. H. and Harder R. L. 'A proposed standard set of problems to test finite element accuracy'. *Finite Elements in Analysis and Design*, 1(1985):3–20.

Nagtegaal J. C. and Fox D. D. 'Using assumed enhanced strain elements for large compressible deformation'. *Int. J. Sol. Struct.*, 33(1996):3151–3159.

Nilsson C. 'On nonlocal rate-independent plasticity'. *Int. J. Plast.*, 14(1998):551–576.

Puso M. A. 'A highly efficient enhanced assumed strain physically stabilized hexahedral element'. *Int. J. Num. Meth. Engrg.*, 49(2000):1029–1064.

Shu J. Y. and Barlow C. Y. 'Strain gradient effects on microscopic strain field in a metal matrix composite.'. *Int. J. Plast.*, 16(2000):563–591.

Simo J. C. , Armero F. and Taylor R.L. 'Improved versions of assumed enhanced strain tri-linear elements for 3D finite deformation problems'. *Comp. Methods Appl. Mech. Engrg.*, 110(1993):359–386.

Simo J. C. and Rifai M. S. 'A class of mixed assumed strain methods and the method of incompatible modes'. *Int. J. Num. Meth. Engrg.*, 29(1990):1595–1638.

Stolken J. S. and Evans A. G. 'A microbend test method for measuring the plasticity length scale.'. *Acta Matter*, 49(1998):5109–5116.

Strömberg L. and Ristinmaa M. 'FE-formulation of non-local plasticity theory'. *Comp. Methods Appl. Mech. Engrg.*, 136(1996):127–144.

Wriggers P. and Reese S. 'A note on enhanced strain methods for large deformations'. *Comp. Methods Appl. Mech. Engrg.*, 135(1996):201–209.

Zhu Y. Y. and Cescotto S. 'Unified and mixed formulation of 8-node hexahedral elements by assumed strain method'. *Comp. Methods Appl. Mech. Engrg.*, 129(1996):177–209.

Zupan D. and Saje M. 'The linearized three-dimensional beam theory of naturally curved and twisted beams: the strain vectors formulation'. *Comp. Methods Appl. Mech. Engrg.*, 195(2006):4557–4578.

List of Figures